AMERICAN SOCIETY FOR MICROBIOLOGY | mSystems

Microbial Ecology | Research Article

Environmental matrix and moisture influence soil microbial phenotypes in a simplified porous media incubation

Josué Rodríguez-Ramos,[1] Natalie Sadler,[1] Elias K. Zegeye,[1] Yuliya Farris,[1] Samuel Purvine,[1] Sneha Couvillion,[1] William C. Nelson,[1] Kirsten S. Hofmockel[1]

AUTHOR AFFILIATION See affiliation list on p. 20.

ABSTRACT Soil moisture and porosity regulate microbial metabolism by influencing factors, such as system chemistry, substrate availability, and soil connectivity. However, accurately representing the soil environment and establishing a tractable microbial community that limits confounding variables is difficult. Here, we use a reduced-complexity microbial consortium grown in a glass bead porous media amended with chitin to test the effects of moisture and a structural matrix on microbial phenotypes. Leveraging metagenomes, metatranscriptomes, metaproteomes, and metabolomes, we saw that our porous media system significantly altered microbial phenotypes compared with the liquid incubations, denoting the importance of incorporating pores and surfaces for understanding microbial phenotypes in soils. These phenotypic shifts were mainly driven by differences in expression of *Streptomyces* and *Ensifer*, which included a significant decrease in overall chitin degradation between porous media and liquid. Our findings suggest that the success of *Ensifer* in porous media is likely related to its ability to repurpose carbon via the glyoxylate shunt amidst a lack of chitin degradation byproducts while potentially using polyhydroxyalkanoate granules as a C source. We also identified traits expressed by *Ensifer* and others, including motility, stress resistance, and carbon conservation, that likely influence the metabolic profiles observed across treatments. Together, these results demonstrate that porous media incubations promote structure-induced microbial phenotypes and are likely a better proxy for soil conditions than liquid culture systems. Furthermore, they emphasize that microbial phenotypes encompass not only the multi-enzyme pathways involved in metabolism but also include the complex interactions with the environment and other community members.

IMPORTANCE Soil moisture and porosity are critical in shaping microbial metabolism. However, accurately representing the soil environment in tractable laboratory experiments remains a challenging frontier. Through our reduced complexity microbial consortium experiment in porous media, we reveal that predicting microbial metabolism from gene-based pathways alone often falls short of capturing the intricate phenotypes driven by cellular interactions. Our findings highlight that porosity and moisture significantly affect chitin decomposition, with environmental matrix (i.e., glass beads) shifting community metabolism towards stress tolerance, reduced resource acquisition, and increased carbon conservation, ultimately invoking unique microbial strategies not evident in liquid cultures. Moreover, we find evidence that changes in moisture relate to community shifts regarding motility, transporters, and biofilm formation, which likely influence chitin degradation. Ultimately, our incubations showcase how reduced complexity communities can be informative of microbial metabolism and present a useful alternative to liquid cultures for studying soil microbial phenotypes.

Editor Marcela Hernandez, University of East Anglia, Norwich, United Kingdom

Address correspondence to Kirsten S. Hofmockel, kirsten.hofmockel@pnnl.gov.

Josué Rodríguez-Ramos and Natalie Sadler contributed equally to this article. Author order was determined based on who had the most time to address edits in final manuscript.

The authors declare no conflict of interest.

See the funding table on p. 20.

Received 2 December 2024
Accepted 16 January 2025
Published 24 February 2025

This is a work of the U.S. Government and is not subject to copyright protection in the United States. Foreign copyrights may apply.

KEYWORDS model soil microbial community, metagenomics, metaproteomics, metatranscriptomics, carbon use efficiency, chitin metabolism, soil microbiology, soil moisture, glyoxylate shunt, microbial stress response

To accurately understand the impact of environmental changes, such as drought on terrestrial carbon cycling, it is crucial to understand their effects on soil microbiome function. However, heterogeneity in the biological, chemical, and physical properties of soil adds layers of complexity to understanding microbial organic matter (OM) decomposition. For example, soil particles and aggregates offer surface area and form a porous matrix with varying aqueous conditions, ranging from saturated pore spaces to films too narrow for microbial movement (1). Further, porosity allows for compartmentalization and the privatization of goods (e.g., enzymes, osmolytes, and vitamins) which translates to an expanded range of functional niches and increased diversity of organisms, functions, and metabolites, all of which in turn can alter interspecies competition (2). However, while the role of environmental matrices and moisture in shaping the soil microbiome is well acknowledged (3), mechanistic, genome-resolved details on how microbial communities alter their metabolism in response to these environmental changes are less studied. As such, there is a critical need for methods that enable scientists to interrogate changes at community and organismal levels.

Chitin is the key structural component for fungal cell walls, protists, and insect exoskeletons and is the second most abundant biopolymer found on the planet, following cellulose (4, 5). Unlike cellulose, chitin is composed of carbon and nitrogen and, therefore, represents an essential elemental cycling hub (6). Like many polymers comprising soil OM, chitin is an insoluble substrate that requires enzymatic depolymerization into small subunits before microbial assimilation. As such, chitin decomposition rates are influenced by the effects that moisture can have on microbial metabolism. These metabolic shifts can occur because soil moisture regulates ecosystem characteristics, like habitat connectivity, microbial mobility, and substrate diffusion (7–9), which ultimately influence changes in microbial strategies for yield (often measured as carbon use efficiency [CUE]), resource acquisition (the production of extracellular enzymes, transporters, and motility), and/or stress response (e.g., oxygen stress, drought stress, etc.) (10). The chitin degradation phenotype requires the coordinated expression and deployment of a suite of enzymes for polymer hydrolysis (i.e., a resource acquisition). These enzymes include extracellular, cell tethered, or intracellular proteins, such as genes within auxiliary activity family 10 (AA10,; chitin monooxygenase, previously CBM33), glycoside hydrolase family 18/19 (GH18/19; chitinase), and a range of enzymes involved in chitin oligomer/monomer transport and metabolism (11). Ultimately, these characteristics make chitin a useful carbon source for identifying shifts in microbial lifestyle strategies. However, identifying how the strategies of microbial populations contribute to community decomposition in spatially heterogeneous environments remains a challenging frontier for soil ecology.

Extrapolating from an organism's genetic code to its observable phenotypes is regarded as the "holy grail" of genomics research (12). However, microbial community phenotypes can often result from multiple complementary processes that can be difficult, and sometimes impossible, to measure accurately. These properties are described as emergent properties, meaning that they cannot be wholly predicted from the observations of the constituent components to the overall unit or process (13, 14), and instead are the result of a combination of factors. Examples of these emergent properties include substrate uptake involving multiple genes (14) and shifts in bacterial lifestyle strategies between high yield, resource acquisition, and stress tolerance in response to nutrient limitation or changing environmental conditions (10). Due to these emergent properties, inferring phenotypes based on the presence of specific key genes often fails to predict complex phenotypes that arise from cellular interactions like biofilm production and organismal metabolic handoffs, all of which can significantly alter community OM decomposition. As such, a comprehensive metabolic accounting beyond

just "key" genes of specific processes is often required to fully understand microbial community dynamics, but the overwhelming heterogeneity of soil makes this difficult.

Here, we present a mechanistic, genome-resolved overview of the impacts that the environmental matrix and moisture have on chitin decomposition by using a tractably complex microbial community. Specifically, we aimed to examine how the environmental matrix and moisture influence community structure, metabolism, and overall respiration. To achieve our goal, we used a soil-derived microbial community (15) in either broth culture or porous glass bead incubations at three different moisture levels (100%, 50%, and 25% moisture saturation) (Fig. 1).

MATERIALS AND METHODS

Soil extract preparation and characterization

The soil extract was prepared by mixing 500 g of sieved (2 mm sieve) soil from the Tall Wheatgrass Irrigation Field Trial in Prosser, WA, with 1 L of Milli-Q water. The soil slurry was shaken at 160 RPM for 48 h at 4°C. The slurry was then centrifuged at 12,000×*g* for 30 min. Next, the supernatant (soil extract) was filter sterilized using a 0.22 µm vacuum filtration unit and stored at 4°C. The total C/N and elemental composition was determined by VarioTOC analyzer (Elementar, Langenselbold, Germany) for five replicates. The average total C was 48.52 µg/mL, and the average total N was 10.18 µg/mL for the soil extract.

Cultivation and preparation of model soil consortia 1 (MSC-1) inoculum

The model soil consortia (MSC) contain approximately 40 species that were enriched from native soil, using chitin as a sole carbon source (15), whose community interactions have been extensively studied (16, 17). MSC-1 inoculum was prepared by first cultivating the cells from glycerol stock on chitin–soil extract agar plates. To prepare chitin–soil extract agar plates for starting MSC-1 cultures, soil extract, 0.1% chitin (Bean Town Chemical), and 1.5% agar (BD Difco) were mixed and autoclaved 120°C for 15 min. For each 100 mm plate, 25 mL of chitin–soil extract agar solution was poured and allowed to cool at room temperature until solidified. Each plate was streaked with 200 µL of MSC-1 glycerol stock and incubated at 20°C in the dark for 7 days, per the original published work with MSC (15). On the 7th day, the biomass was collected and transferred to a 50 mL conical tube. The cell pellets were suspended with 1× sterile phosphate buffer saline (PBS), centrifuged at 7,000 × *g* for 5 min, and the supernatant was removed. Sterile soil extract enriched with 1,000 ppm chitin and 600 ppm glucose was then used to dilute the biomass to achieve an OD_{600} of 0.09 (15).

Incubation preparation, incubation, and respiration measurements

We used four styles of microcosms to test for structure- and moisture-induced differences in community growth and phenotypes. These include liquid media "broth" microcosms and structured porous media microcosms composed of glass and polyacrylamide beads with varying amounts of liquid media applied to achieve 20%, 10%, or 5% liquid to bead (wt/wt), which translates to 100%, 50%, and 25% moisture saturation. Then, 100% moisture saturation was determined by the weight of the liquid it took to fill the pore spaces between the bead matrix until it reached the uppermost bead layer within the microcosm. To test structure, we prepared broth microcosms by adding 3 mL of sterile water and 1 mL of soil extract carrying MSC-1 inoculum prepared as described above to sterile 30 mL serum bottles. The same volume of water and soil extract inoculum was added to 30 mL serum bottles with a porous media matrix composed of 16 g of mixed size glass beads (2.7 [10 g], 1.00 [4 g], and 0.1 [2 g] mm diameter beads). In addition to the glass beads, 0.1 g of 45–90 µm polyacrylamide beads (Bio-Gel P-6, BioRad) were added to uniformly distribute the moisture throughout the porous media. To test varying moisture levels, we also prepared 50% and 25% moisture-saturated incubations. The 50%

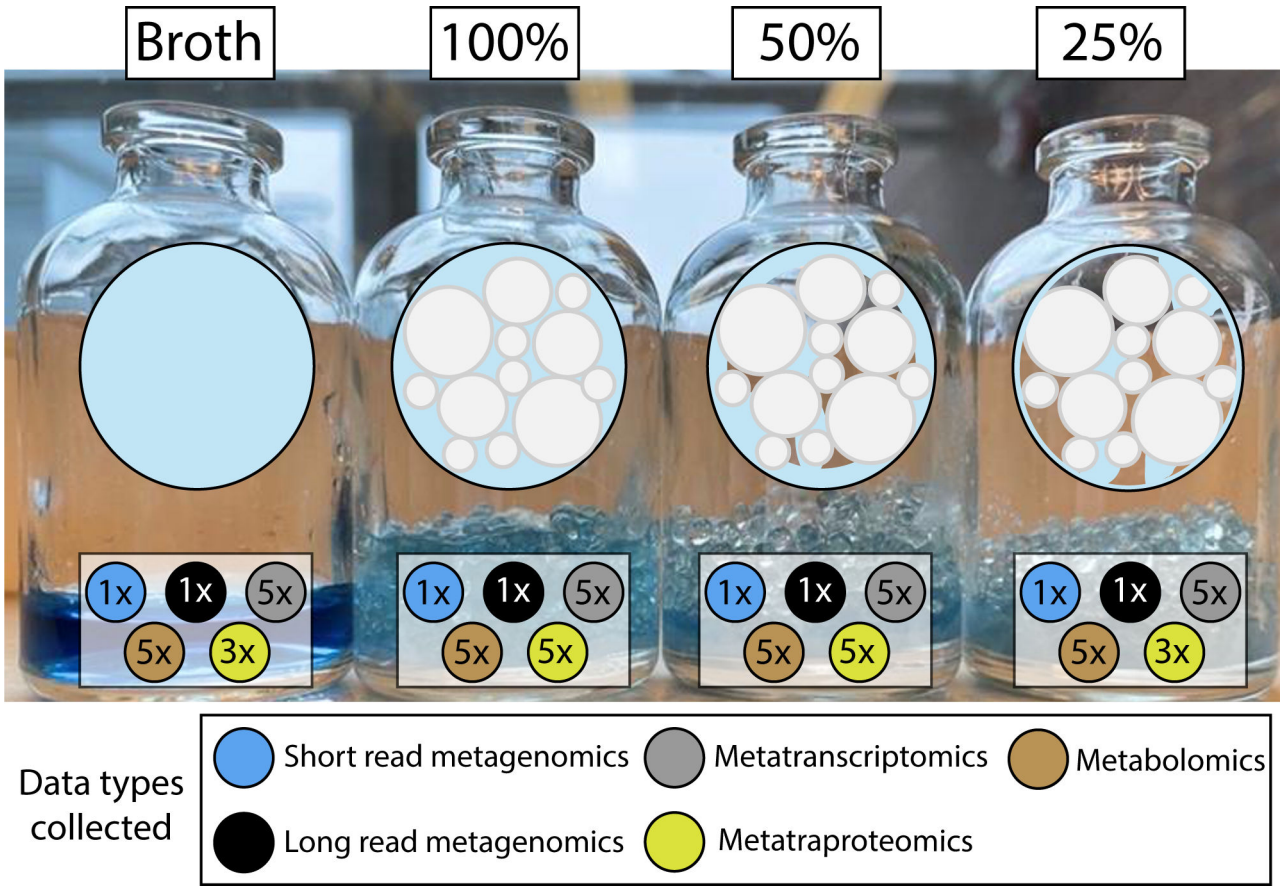

FIG 1 A multi-omic approach for understanding reduced-complexity microbial community dynamics upon structure and moisture gradients. Overview of the experimental design that denotes the total number of samples that were collected per treatment type. The first bottle contains a liquid culture that is fully saturated, and the second bottle contains 100% saturation with porous media composed of glass beads. The third and fourth bottles represent a decrease in moisture gradient. Circles below each bottle denote data types collected.

and 25% saturated incubations had equivalent amounts of glass beads, polyacrylamide beads, and soil extract MSC-1 inoculum as the 100%, but the 50% received only 1 mL of sterile water, and the 25% received no addition water (Fig. 1). Prior to inoculation, the serum bottles and beads were heat sterilized (121°C for 45 min), cooled to room temperature, and inoculated with 1 mL of soil extract liquid enriched with 1,000 ppm chitin, 600 ppm glucose, and MSC-1 cells adjusted to an OD_{600} of 0.09. In total, each sample received 722.92 µg of C (434.4 µg from chitin, 240 µg from glucose, and 48.53 µg from soil extract) and 73.48 µg of N (63.3 µg from chitin and 10.18 µg from soil extract), yielding a C:N ratio of 9.84:1. Next, sterile water was added as previously described. Bottles were weighed and then incubated at 28°C for 4 days. An additional five replicates for each treatment were also incubated for 8 days to continue monitoring respiration. Scaling up the size of our microcosms to eliminate the need for composite samples was desirable but not easily achieved. We were limited to commercially available airtight glassware (requirement for sampling gas from the microcosm headspace for CO_2 analysis; see below) and wanted to maintain a shallow bead matrix to prevent our cultures from quickly entering an anoxic state. For a broader context on the history of porous media incubations, please see the supplemental methods and results.

Respiration for five representative replicates from each treatment was measured daily. To do so, 10 mL of head space gas was collected from incubations by 20 mL gastight syringe. The headspace gas was then injected in to and measured by EGM-4 PP infrared CO_2 analyzer. Incubations were transferred to a sterile biological safety cabinet, and septa were removed to allow for headspace gas exchange for 30 min. Incubation bottles

were then re-capped with septum and aluminum collar. The CO_2 concentrations were calculated against the calibration standard gas (CO_2 2,000 ppm). Concentrations were corrected for the CO_2 dissolution in liquid media (18), and effluxes were calculated from the slope of the linear regression between CO_2 concentration and incubation time. Respiration rate was calculated as corrected CO_2 concentration divided by the time between the headspace atmosphere exchange and the measurement. The µg of C from µg of CO_2 was determined by calculating as 27.29% of CO_2 elemental mass. Cumulative respired C (µg C) was calculated by averaging the respiration rate between adjacent measurement dates, multiplying by the interval between them, and summing the C respired between each rate measured.

Sample harvesting, subsampling, and preparation

After 4 days of incubation, samples were harvested for analysis. To generate enough biomass for metagenomic sequencing and multi-omic sample preparations, 20 replicate microcosms for each of the four treatments were prepared and then pooled to create five representative composite samples (one composite = 5 pooled microcosms). The liquid content of each sample replicate bottle was transferred to 50 mL conical collection tubes. Next, 2 mL of 2-(N-morpholino)ethanesulfonic acid (MES) buffer (pH 6) was added to the bead matrix and vortexed for 10 s to suspend cells. The cell suspension was transferred to the corresponding collection tubes, and this step was repeated once more with an additional 2 mL of MES buffer. The harvested and pooled samples were split into two aliquots. The first was comprised of 85% of the pooled sample volume, which was used for downstream proteomic sample processing, while the remaining 15% of the sample volume was used for DNA/RNA extraction and extracellular metabolomic sample processing. The 85% and 15% volume sample aliquots were centrifuged at 5,000× g for 10 min to pellet cells. The 15% volume cell pellets and supernatants were separated. Cell pellets were flash frozen with liquid N_2 for nucleotide extraction, and the supernatants were flash frozen in a separate tube for metabolite extractions. The 85% volume samples were kept on ice or at 4°C for metaproteomic sample preparation.

The supernatant from the 85% samples was concentrated and buffer exchanged with fresh MES buffer using 30 kDa molecular weight cutoff centrifugation filters with polyethersulfone membranes (Millipore). The washed extracellular proteins were then resuspended in 0.5 mL MES buffer and transferred to 1.5 mL conical tubes. Meanwhile, the 85% sample cell pellets were transferred with 0.5 mL of MES buffer to 2 mL mechanically resistant tubes holding 100 µL of zirconium beads (100 µm diameter, Biospec). The cells were then lysed by bead beating (1 min at 6 m/s, rest 5 min, 3×). The 85% vol sample lysates and concentrated supernatants were then combined, and protein was quantified by CBQCA protein quantification kit assay (ThermoFisher) as described by the manufacturer with each sample run in triplicate using 5 µL per technical replicate and quantified using a Biotek Synergy H1 plate reader with 465 nm excitation and 550 nm emission. Protein (µg) was adjusted to represent µg of carbon in biomass by using a 53% conversion factor for the average theoretical elemental composition for protein (19), followed by a 55% conversion factor to represent the proportion of biomass that is estimated to be protein (20). The supernatants from the 15% vol collection were thawed on ice, and 1.5 mL was filtered using 0.22 µm syringe filters (Pall Corps) and transferred to 1.5 mL tubes. The samples were then covered with BreatheEasier membranes, flash frozen in liquid N_2, and then lyophilized until dry.

Metagenome extraction, assembly, and data processing

The cell pellets from the 15% vol fraction were collected. ZymoBIOMICS DNA/RNA mini prep kit was used for co-extracting both pools of nucleotides. RNA/DNA was quantified by Qubit assay, and purity was checked by NanoDrop (absorbance ratios of 260 nm/280 nm and 260 nm/230 nm). Samples were shipped on dry ice to be analyzed. Both short-read and long-read sequences were processed at the Joint Genome Institute (JGI) with Illumina and PacBio CCS sequencers, respectively. Long-read metagenomes were

fully assembled and processed using the JGI workflow (21) and downloaded from the JGI Data Portal. Interleaved, short-read sequences were downloaded from the JGI Data Portal and trimmed with bbduk (22) to ensure high-quality reads using parameters ktrim = r k = 23 mink = 11 hdist = 1 qtrim = rl trimq = 20, and minlength = 75, per the JGI standard workflow (21). Trimmed reads were subsequently assembled with MEGAHIT (23) using default settings. Ribosomal contamination was removed by identifying ribosomal RNA using barrnap (24) and removing reads that mapped to the identified rRNA reference database.

Bacterial metagenomic binning, quality control, annotation, and taxonomy

Metagenome assembled genomes (MAGs) were generated using both the standard JGI workflow (long-read sequencing) (21) and metaWRAP (short-read sequencing) (25). For short-read metagenomes, scaffolds ≥ 2,500 bp were extracted using seqkit (26) and binned using the MetaWrap binning and refinement modules with default settings. After binning, MAGs from both short-read and long-read metagenomes were pooled and processed together. To ensure only quality MAGs, any MAGs that were not medium quality (MQ; ≥50% complete, <10% contaminated) or high quality (HQ; >90% complete, <5% contaminated) per MIMAG standards (27) were discarded from subsequent analyses, resulting in 174 MAGs. These MAGs were subsequently dereplicated at 99% identity, yielding 29 MAGs. MAG and sample statistics can be found in Table S1.

These 29 MAGs were functionally annotated using DRAM (28) and eggNOG (29), with full annotations hosted on PNNL DataHub (https://doi.org/10.25584/2476507), and summarized in the supplemental methods and results, Table S2, and Table S3. Aside from DRAM-assigned cutoffs for the genomic potential of metabolisms, we employed additional cutoffs described in the supplemental methods and results for assigning potential.

For taxonomic classification, we used the Genome Taxonomy Database (GTDB) toolkit version 2.3.2 using the r214 database in October 2023 (30, 31). PSORTb web-based GUI was used to localize chitinase enzymes of interest (32). All supplemental code used to generate these data are hosted on GitHub (https://github.com/jrr-microbio/MSC1_SSA_incubations_moisture).

Genome relative abundances (metagenomics) and relative expression (metatranscriptomics)

To determine the relative abundance and expression of our MAGs, metagenomic and metatranscriptomic data sets were mapped to a reference database of the 29 MQ/HQ MAGs using bbmap from the bbtools suite (22). To remove ribosomal RNA (rRNA) contamination from metatranscriptomes, reads were mapped to a database of rRNA from our assembled metagenomes identified using barrnap (24) with flags ambiguous = all and perfectmode = t. Reads that perfectly mapped to rRNA were then removed, and subsequent cleaned reads were used. Both cleaned metatranscriptomic reads and metagenomic reads were mapped to our MAG database using bbmap with flag ambiguous = all. After initial mapping, sequence alignment map (SAM) files were then filtered to report hits of ≥98% identity (minidfilter = 0.98), and only primary mappings (pimaryonly = t) using reformat.sh from bbsuite (22). Metagenomic reads were additionally filtered to include only paired mapping results (paired = true). Metagenomic mapping SAM files were processed with CoverM (33) and normalized using the transcripts per million (TPM) calculation (for gene and library size), a minimum contig coverage of 75%, and a minimum depth coverage of 2×. Metatranscriptomic mapping SAM files were processed with featureCounts (34) using the subread package from Bioconda (35). Genes of the 29 MAG database were called using DRAM (28), and the resulting .gff file was used for featureCounts along with flags -t rrna, trna, CDS, -s 2 (reversely stranded), -M (multi-map), and -p (paired). The resulting counts were then normalized in R to the total length of each respective gene and subsequently converted

to transcripts per million (TPM) according to the code in Additional File 4 of the geTMM manuscript (36).

Raw counts for the read mapping that met minimum contig coverage cutoffs were used for DESEQ2 package in R (37), with adj. $P \leq 0.05$ reported (Table S4). For NMDS of metatranscriptomic data, normalized TPM values for each MAG were used as input in R for metaMDS from the vegan library (38). Normalized TPM values for each MAG were also used for sparse partial least squares regressions (sPLS) (39). All R plots were made in R using ggplot2 (40), and others with RawGraphs (41). All supplemental codes used to generate these data are included hosted on GitHub (https://github.com/jrr-microbio/MSC1_SSA_incubations_moisture). Read mapping results can be found in Table S1 and DESEQ2 raw results are in Table S4.

Metaproteome generation and peptide mapping

Aliquots of 100 µg of each protein sample were denatured with 8M urea and reduced by incubating at 60°C for 30 min with 500 mM dithiothreitol. Samples were then alkylated by incubating with 40 mM iodoacetamide at 37°C for 60 min. Digestion was performed using 1:50 ratio of trypsin (Promega, Madison, WI, USA) to protein and incubated for 3 h at 37°C. Digested peptides were loaded on C18 SPE columns, preconditioned with MeOH and equilibrated with 0.1% trifluoroacetic acid (TFA). Samples were washed with a solution of 5% acetonitrile (ACN) and 0.1% TFA and eluted with a solution of 20% ACN and 0.1% TFA. Eluted peptides were dried by speed vacuum and reconstituted in 25 mM NH_4HCO_3 (pH 8), and the concentrations were normalized to 0.1 g L^{-1} for analysis.

Peptides were analyzed using a custom-built reversed-phase LC column coupled to a LTQ Orbitrap Velos mass spectrometer (Thermo Fisher). The raw spectra from the MS were extracted using MSConvert (part of the Proteowizard tool suite (42), and precursor m/z values were re-calibrated using MZRefinery (43) and searched against the genes of all long-read and short-read metagenomes using MS-GF+ (41) in target-decoy mode (44). MS-GF+ Q-values were used to calculate the FDR value (~0.01 cutoff). Peptide-to-protein relationships were established using parsimony, such that only non-unique peptides belonging to more than one uniquely identified protein were not used for further quantitation.

Detected metaproteome peptides were then mapped back to the genes from our total metagenomic assemblies reporting all possible hits. Results from the peptide matching of total metagenomic gene content were then subset to only those genes that were present within our 29 MAG database when peptides were confidently assigned to one or more genes, and subsequent analyses were performed on this subset. Metaproteomic counts were subsequently converted to spectral abundance factors (SAFs) by calculating the length of each protein and normalizing by total counts per sample (NSAF). For NMDS of metaproteomic data, normalized NSAF values for each MAG were used as input in R for metaMDS from the *vegan* library (38). Raw metaproteomic counts as well as the NSAF normalized values for the database of 29 MAGs are shown in Table S1.

Extracellular LC–MS/MS metabolite processing

Extracellular metabolites were analyzed using reverse phase (RP) and hydrophilic interaction chromatography (HILIC) separations on a Thermo Fisher Scientific Q Exactive Plus mass spectrometer (Thermo Scientific, San Jose, CA) coupled with a Waters Acquity UPLC H class liquid chromatography system (Waters Corp., Milford, MA). Metabolites were brought up in 100 µL of 80% LCMS grade methanol and 20% nanopure water, vortexed to mix, and centrifuged at 4,500 rpm for 5 min. The wells of a 0.2 µm PTFE 96 well filter plate were preconditioned with methanol and then placed on top of a 96-well collection plate. Samples were then transferred to the filter plate wells, and N_2 was applied at 9 psi via a CEREX System 96 processor for positive pressure SPE to push the sample through the filtered well plate into the collection well plate.

RP separation was performed by injecting 5 µL of sample onto a Thermo Scientific Waters Acquity UPLC BEH C18 column (130 Å, 1.7 µm, 2.1 mm ID × 100 mm L) preceded

by a Acquity UPLC BEH C18 Vanguard Pre-Column (130 Å, 1.7 µm, 2.1 mm ID × 5 mm L) heated to 40°C. Metabolites were separated using a 15 min gradient, with data collected on the first 10 min. For RP acquisition, positive mode polarity was run. The gradient used was identical, but the solvent composition was different between the modes. The positive mode mobile phase A consisted of 0.1% formic acid in nanopure water ,with the mobile phase B consisting of 0.1% formic acid in LCMS grade methanol, while the negative mode mobile phase A consisted of 6.5 mM ammonium bicarbonate in nanopure water at a pH of 8, with the mobile phase B consisting of 6.5 mM ammonium bicarbonate in 95% LCMS grade methanol and 5% nanopure water. The gradient used was as follows (min, flowrate in mL/min, %B): 0,0.35,5; 4,0.35,70; 4.5,0.35,98; 5.4,0.35,98; 5.6,0.35,0.5; 15,0.35,0.5. HILIC separation was performed by injecting 3 µL of sample onto a Waters Acquity UPLC BEH Amide column (130 Å, 1.7 µm, 2.1 mm ID × 100 mm L) preceded by a Acquity UPLC BEH Amide Vanguard Pre-Column (130 Å, 1.7 µm, 2.1 mm ID × 5 mm L) heated to 40°C.

Metabolites were separated using a 21 min gradient, with data collected for the first 16 min. For HILIC mode, both positive and negative spray ionizations were used in separate injections using the same mobile phase compositions. The HILIC mobile phase A used consisted of 0.125% formic acid and 10 mM ammonium formate in nanopure water with a mobile phase B consisting of 0.125% formic acid and 10 mM ammonium formate in 95% LCMS grade acetonitrile and 5% nanopure water. The gradient used was as follows (min, flowrate in mL/min, %B): 0, 0.4, 100; 2, 0.4, 100; 5, 0.4, 70; 5.7, 0.4, 70; 7, 0.4, 40; 7.5, 0.4, 40; 8.25, 0.4, 30; and 10.75, 0.4, 100. For both RP and HILIC separations, the Thermo Fisher Scientific Q Exactive was equipped with a HESI source and high flow needle with the following parameters: spray voltage of 3.6 kV in the positive mode and 3 kV in the negative mode, capillary temperature of 350°C in the positive mode and 275°C in the negative mode, aux gas heater temp of 325°C in the positive mode and 300°C in the negative mode, sheath gas at 45 L/min in the positive mode and 30 L/min in the negative mode, auxiliary gas at 15 L/min in the positive mode and 25 L/min in the negative mode, and spare gas at 1 L/min in the positive mode and 2 L/min in the negative mode. Metabolites were analyzed at a resolution of 70 k and a scan range of 70 to 1,000 *m/z* for parent ions, followed by MS/MS HCD fragmentation which is data dependent on the top four ions with a resolution of 17.5 K and stepped normalized collision energies of 20, 30, and 40. All metabolite data are available in Table S5.

Metabolomics data analysis

Metabolite identifications were made using MS-DIAL (45) v4.92 for peak detection, identification, and alignment. The experimental data were matched both to in-house libraries (*m/z* less than 0.003 Da, retention time less than 0.3 min, MS/MS spectral match) and a compilation of publicly available MS/MS databases (*m/z* less than 0.003 Da, MS/MS spectral match) available in MS-DIAL. The tandem mass spectra and corresponding fragment ions, mass measurement error, and aligned chromatographic features were manually examined to remove false positives. Relative quantification was performed by calculating peak areas on extracted ion chromatograms of precursor masses. Features detected in at least three of the five replicates were retained.

Statistical analyses

All statistical analyses were performed with the TPM-normalized or NSAF-normalized values described above. To determine the overall composition of our microbial community across treatments, we calculated Bray–Curtis dissimilarities using vegan (38) in R, and these were visualized using nonmetric multidimensional scaling (NMDS) with k = 2. For each treatment type, MANOVA analyses were then performed using the adonis2 function from vegan. To identify differentially expressed genes, raw counts that met the 75% alignment fraction and 2× coverage were input into DESeq2 in R (37). Samples were split into two treatments: structure comparisons and moisture comparisons. The subset of moisture comparison samples that were compared were those corresponding

to 5% and 25% moisture. DESeq2 was then run on each subset of samples separately. To identify which genomes were strongly related to the collected metabolites, we used sparse partial least square regressions (sPLS) (39) on the metatranscriptomic expression patterns of the structure and moisture sample subsets. For metabolism-level differential expression, all annotations and calls that were used to aggregate groups are denoted in Table S2 and Table S6, and detailed inputs are on GitHub https://github.com/jrr-microbio/MSC1_SSA_incubations_moisture.

Statistical analysis of metabolomics data was performed using the PMart web application (46). Data were $\log_2$-transformed and normalized via global median centering. Statistical comparisons were performed for structure (liquid vs 100% moisture) or moisture (100%, 50%, or 25% moisture) using ANOVA with a Holm test correction (47). For each metabolite, these adjusted *P* values and the mean $\log_2$ fold changes for each of the above comparisons are reported (Table S5), along with the number of observations per group.

RESULTS

Leveraging multi-omics data sets of a reduced complexity microbial community to understand the role of environmental matrix and moisture on community patterns

After a 96 h incubation of our soil-derived microbial community (15) in either liquid or porous media, we sequenced four long-read reference metagenomes, four short-read reference metagenomes, 20 metatranscriptomes, and 16 metaproteomes (Fig. 1). From our short-read and long-read metagenomes (n = 4 short-read, n = 4 long-read), we generated a reference database of 29 metagenome assembled genomes (MAGs) that were medium-quality or greater (average completion = 94.0%, average contamination = 0.4%). Altogether, 19 of our MAGs (66%) were from long-read metagenomes that had ≤3 scaffolds and were 98% complete, and our entire MAG database contained 128,133 genes. While it is likely that there are some lesser abundant strains or species missing from this database due to sequencing depth, our MAGs had species-level representatives of all MSC-2 reduced complexity consortia isolates, which have been extensively characterized as the key organisms for the chitin degradation phenotype (16). Further, the original amplicon sequencing of the MSC-1 community only showed an estimated 30–50 operational taxonomic units (OTUs), and only four are not represented at a genera level by our MAGs (*Bacillus* sp., *Blastococcus* sp., *Inquilinus* sp., and *Massilia* sp.).

To determine if microbial community expression was altered by our treatments, we recruited metatranscriptomic reads and metaproteomic spectra to our reference database of 29 MAGs (Fig. 2; Table S1; see Materials and Methods). Metatranscriptome reads were recruited to 95,756 genes (75% of total), while metaproteomes had spectral hits to 8,627 genes (7% of total). Due to low recruitment in our metaproteomics data, we performed our statistical and metabolic analyses using transcriptomic data. At a community level, overall expression by both metatranscriptomics and metaproteomics showed significant differences between porous media and liquid treatments (metaT: R^2 = 0.86, $P \leq 0.05$, metaP: $R^2 = 0.76$, $P \leq 0.05$) (Fig. S1). Moisture content (100%, 50%, and 25% saturation) also showed a significant effect on community expression (metaT: $R^2 = 0.26$, $P \leq 0.05$). No effect of moisture content was detected in the metaproteome profiles, likely because of data sparsity (metaP: $R^2 = 0.09$, $P > 0.05$). Our results show that while moisture patterns explained less of the variation than the environmental matrix, both structure (i.e., glass beads) and moisture were strong determinants of community expression.

To explain which organisms were causing these community shifts, we interrogated the expression of individual MAGs across treatments (Fig. 2). In the liquid culture, *Dyadobacter* accounted for 62% of metatranscriptomic expression, followed by *Streptomyces* (10% of expression) and *Ensifer* (7% of expression). In the porous media communities, incubations with the highest moisture (i.e., 100% saturation) showed an expression profile of 62% *Ensifer*, 8% *Flavobacterium*, and 6% *Sphingopyxis*. Across the moisture treatments in the porous media, community abundance and expression were similar.

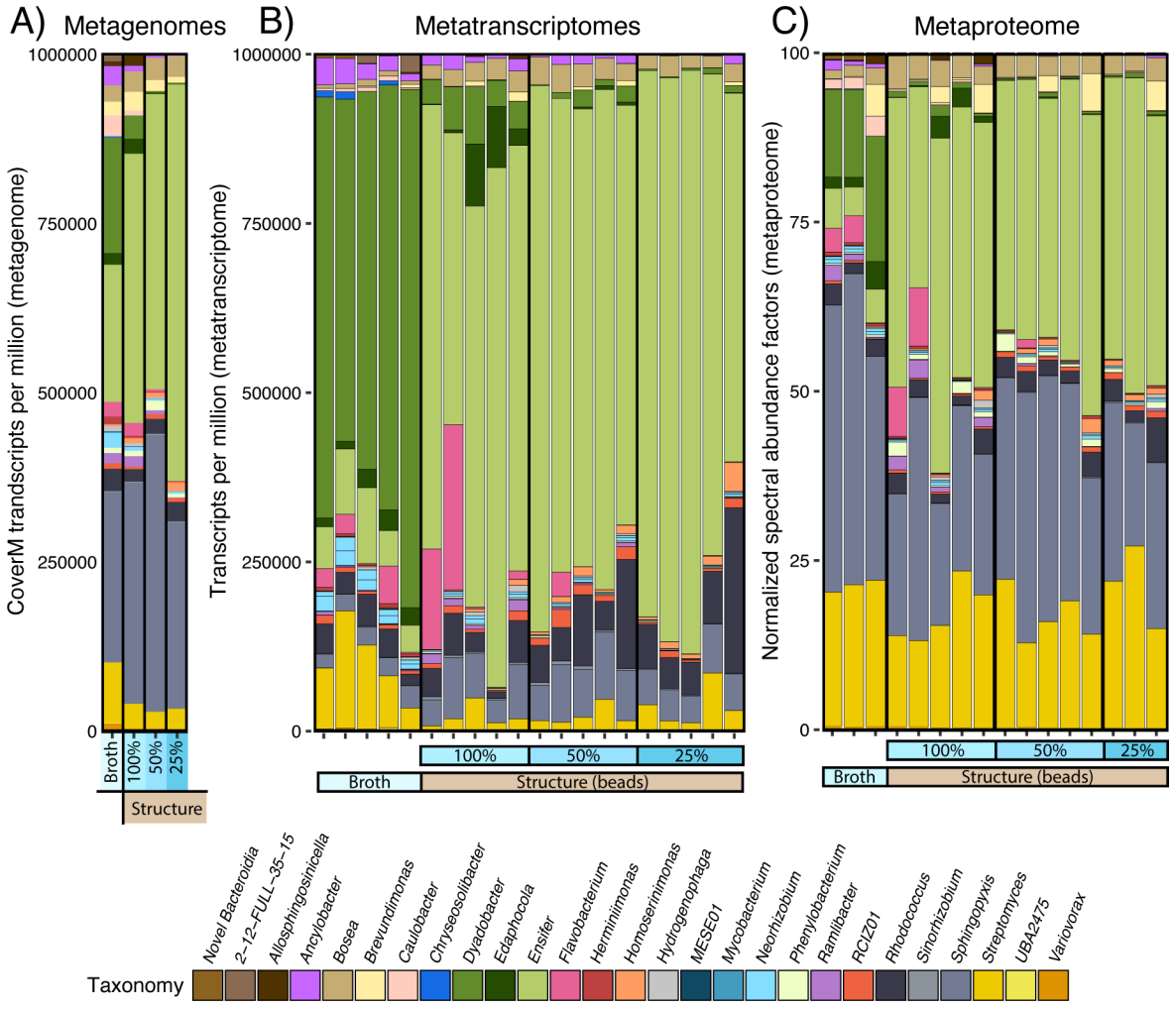

FIG 2 Multiple omics data types highlight different expression patterns across experimental treatments. Stacked bar charts are colored by genera and denote normalized expression (see Materials and Methods) detected by either (A) CoverM trimmed mean of M-values (TMM) normalized metagenomics (n = 5), (B) transcripts per million (TPM) normalized metatranscriptomics (n = 20), or (C) normalized spectral abundance factor (NSAF) metaproteomics (n = 16).

Throughout our incubations, some low abundance members disproportionally contributed to the overall expression pools (i.e., *Streptomyces*, *Dyadobacter*).

Porous media incubations lead to significantly lower chitin metabolism by *Streptomyces*

Changes in chitin decomposition phenotypes were detected via metatranscriptomic activity across our liquid and porous media treatments (Fig. S1). Specifically, we detected high transcriptomic abundance of chitin degradation genes in the liquid treatment, with *Streptomyces* GH18 chitinase being the second most highly expressed carbon degradation gene. In liquid, 89% of chitin metabolism gene expression was assigned to *Streptomyces,* consistent with a central role in resource acquisition (Fig. 3; Table S3). While the capability to degrade chitin and its byproducts is widespread across our MAGs (Fig. 3), the other top four chitindegrading genera in liquid (i.e., *Dyadobacter, Neorhizobium, Ensifer*, and *Sphingopyxis*) together account for only 9% of total chitin degradation expression, and the remaining 22 genera account for less than 1%. While our metaproteomics data set was sparse, it reflected the observed transcriptomic patterns and showed 77% of the expressed peptides for chitin degradation were from *Streptomyces* in the liquid, followed by *Dyadobacter* (12%) and *Sphingopyxis* (11%).

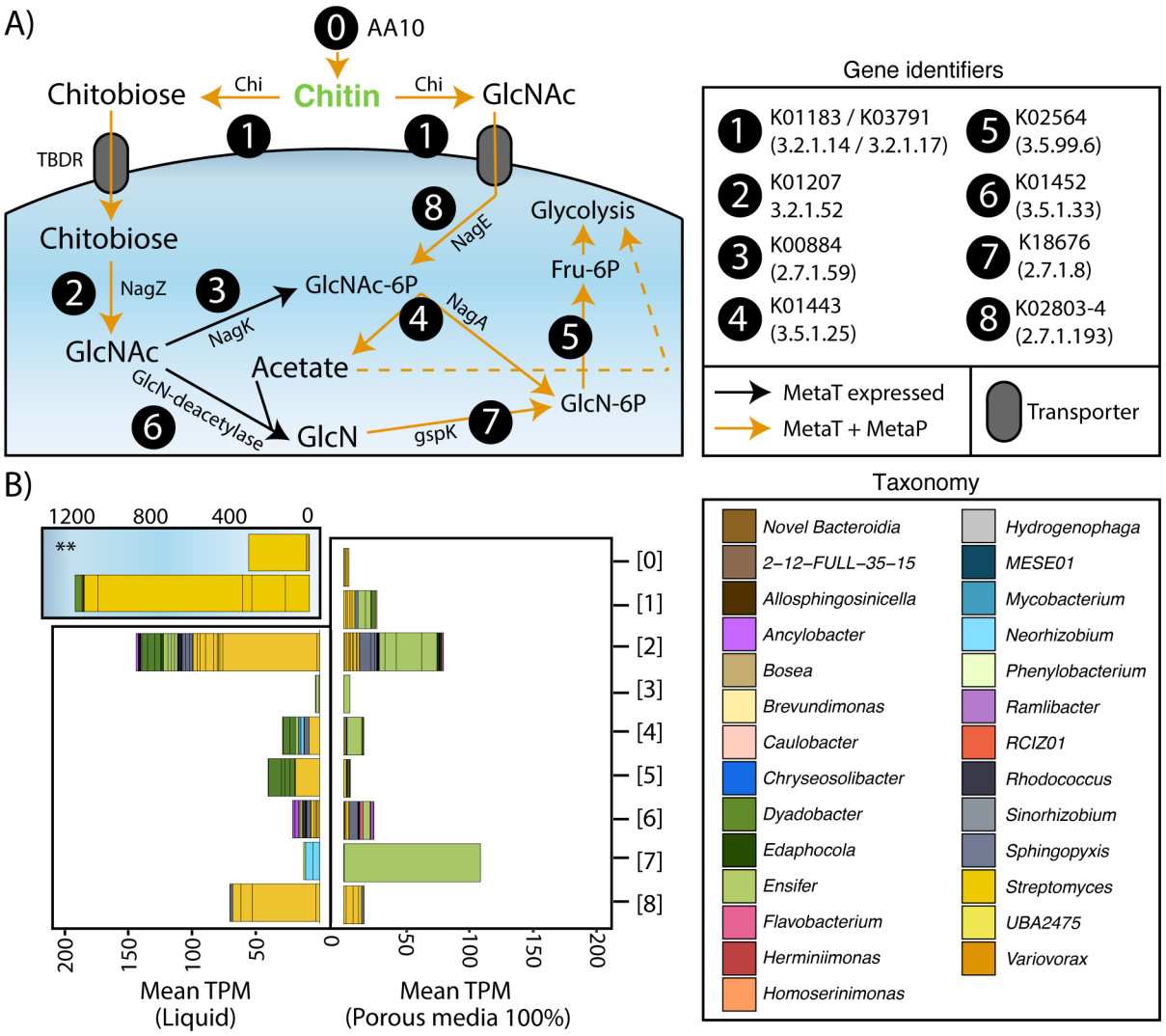

FIG 3 Community members express genes related to chitin degradation. (A) Schematic diagram of a cell shows the overall pathways of chitin degradation in a generic cell. Each gene is represented by a circle and labeled by their KO, common name, and E.C. number. Arrows denote detection in metatranscriptome (black) or both metatranscriptome and metaproteome (orange). The dotted arrow denotes how acetate can be used for glycolysis and downstream metabolisms. (**B**) Butterfly plots denote the mean transcript per million (TPM) across all samples of each of the genes denoted in panel A for either liquid (left) or 100% moisture porous media (right). Colors on stacked bars show genera-level GTDB taxonomy. TBDR = TonB dependent transporter. **Note: axis for "0" (AA10) and "1" (GH18/GH19) is different.

In 100% porous media incubations, the abundance of transcripts related to chitin degradation was significantly lower than in liquid ($P \leq 0.05$). In addition to chitinases, the genes responsible for the linearization of chitin (AA10, lytic polysaccharide monooxygenase) had a 200-fold lower expression in 100% porous media than in liquid culture. *Streptomyces* was the only organism that encoded and transcribed AA10 genes. An extracellular GH18 encoded by *Streptomyces* showed a significantly lower expression in the 100% porous media (base mean = 12,272, $\log_2$ fold change = −8.8, $P \leq 0.05$). Further, all *Streptomyces*-encoded chitinases had significantly lower transcriptomic abundance in 100% porous media (avg. $\log_2$ fold change = −6.5). This suggests that in a structured environment, the role of *Streptomyces* in chitin degradation is reduced. After 4 days, we were unable to detect any expressed genes for the degradation of chitin in the porous media incubations at the same expression level as in the liquid culture. In fact, chitin degradation only accounted for 0.9% of the total transcripts. While overall low in expression, in 100% porous media incubations *Ensifer* took over the largest proportion

(69%) of chitin metabolism, followed by *Streptomyces*, *Sphingopyxis*, *Dyadobacter,* and *Bosea*, which accounted an additional 25% (Tables S3). The remaining 22 MAGs provided only 6% of chitin-related transcriptomic abundance.

Coupled metatranscriptomics and respiration measurements suggest that the glyoxylate shunt likely sustains *Ensifer* cellular carbon needs

Since the overall expression of chitin metabolism genes only comprised a fraction of transcriptomic activity in the porous media, we wanted to understand what other metabolic processes were supplementing microbial community carbon needs. Isocitrate lyase (*aceA* [K01637]) from *Ensifer* was observed to be highly expressed and had significantly higher expression in structured compared with liquid incubations (base mean = 39,980, $\log_2$ fold change = 5.57, $P \leq 0.05$) (Fig. S2). Isocitrate lyase is the first step in the glyoxylate shunt, a carbon conservation mechanism where isocitrate is transformed into glyoxylate and succinate, bypassing the carbon dioxide-generating portion of the TCA cycle (Fig. 4A). Highlighting the overall importance of this metabolism, while the response towards the use of glyoxylate and carbon conservation is mostly expressed by *Ensifer* possibly due to its overwhelming abundance, 19 of the other organisms in MSC-1 (i.e., *Rhodococcus* and *Sinorhizobium*) also encoded isocitrate lyase genes. Further, three of those (*Sinorhizobium*, *Ancylobacter*, and *Phenylobacterium*) had significantly elevated levels of expression in 100% porous media, albeit at possibly negligible levels (avg. base mean = 220, avg. $\log_2$ fold change = 6.76, $P \leq 0.05$). In 100% porous media, *Ensifer* isocitrate lyase showed sixfold higher transcriptomic abundance than any other gene in the TCA cycle (Fig. 4B). *Ensifer* also expressed genes necessary to use the produced glyoxylate to generate 2-phospho-D-glycerate (*gcl* [K01608], *hgy*/*gip* [K01816], *gyaR*/*GOR1* [K00015], and glxK/garK [K00865]), which can ultimately feed into pyruvate for glycolysis. Together, these data suggest that carbon conservation mechanisms via the glyoxylate shunt are likely, supplementing the growth of our microbial consortia in porous media.

Next, we wanted to understand the source of the carbon sustaining this community. The ability to bind polyhydroxyalkanoates (PHA) was encoded by 62% of the organisms. *Ensifer*-encoded phasins (e.g., the granule-associated proteins of PHAs) were the second and third most expressed genes in our entire data set by metatranscriptomics. The two *Ensifer* phasins were also the most expressed genes with significantly higher transcript abundance in structured conditions when compared with liquid culture (avg. base mean = 65,134, $\log_2$ fold change = 4.25, $P \leq 0.05$). These phasins had 67-fold higher expression than the isocitrate lyase from *Ensifer* and 380-fold higher than any TCA cycle gene. While our results also showed that other carbon sources were likely metabolized at the time of sampling (see the supplemental methods and results), it is likely that phasins, carbon storage granules, and the glyoxylate shunt are critical components for survival during stress-inducing conditions. To support our omics-based inferences, we measured respiration rates and overall protein content in each of our samples for each treatment (Fig. S3). In agreement with our carbon conservation hypotheses, porous media incubations produced significantly less CO_2 than liquid samples ($P \leq 0.05$) but yielded nearly equivalent biomass ($P > 0.05$), denoting a higher CUE. This suggests that the porous media community is sustaining its protein production under lower respiration, which supports our hypothesized shift to the glyoxylate shunt.

Lowest moisture levels in porous media incubations demonstrate an increase in metabolisms related to chitin degradation and respiratory processes

While the environmental matrix had the most significant treatment effect, our moisture gradients showed significant differences in overall community expression (Fig. S1 and 4). Across moisture treatments, isocitrate lyase was the functionally annotated gene with the highest expression and had significantly lower expression in low moisture compared with high moisture (base mean = 53,889, $\log_2$ fold change = −28.23). This is likely due to

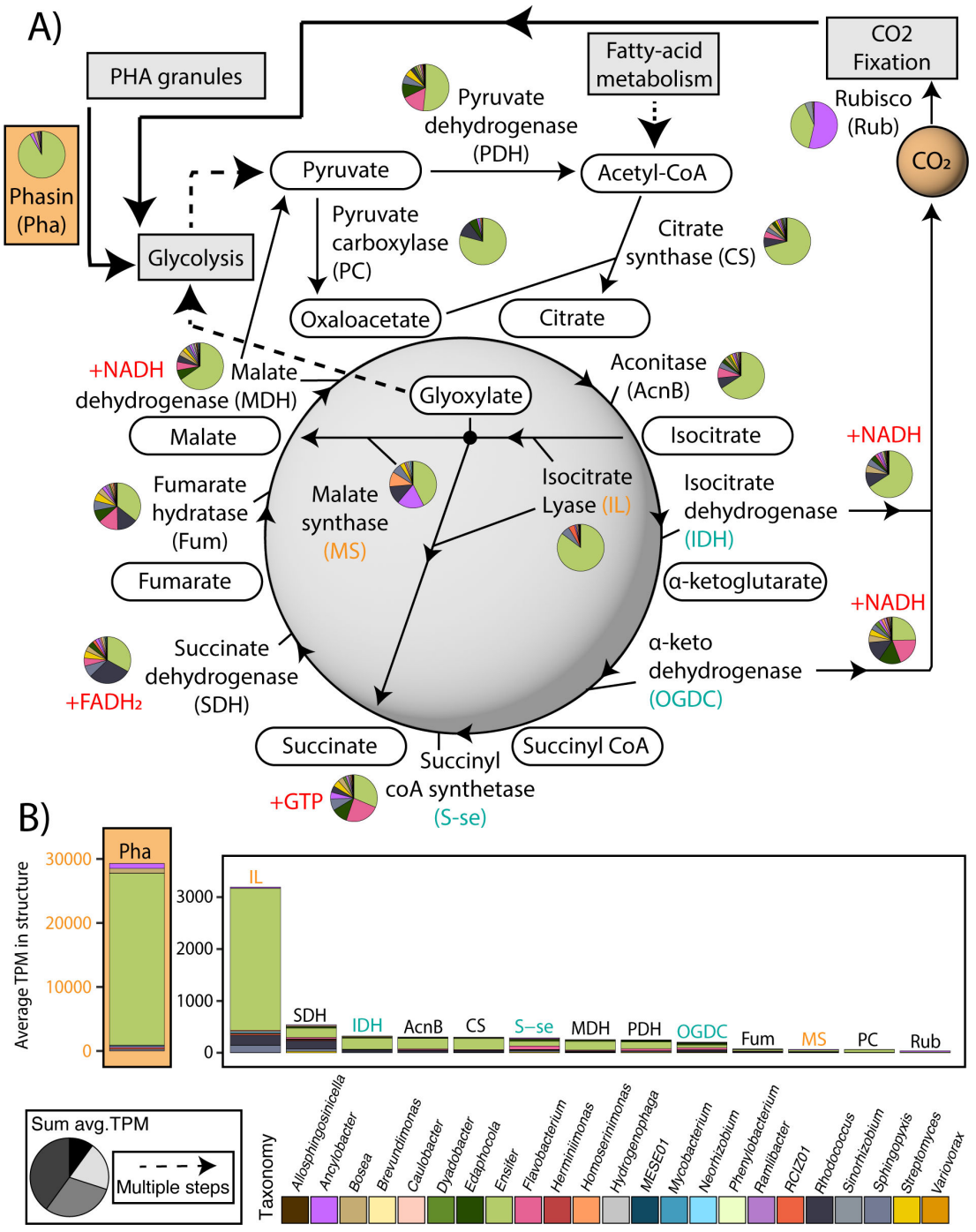

FIG 4 Community-wide transcriptional response in favor of the glyoxylate shunt. (A) Diagram shows the TCA cycle overlaid with the glyoxylate shunt. Pie charts denote the proportion of the summed averages for the structure treatment of each of the genes and are colored by the genera of the organism expressing the gene. (B) Bar charts denote the summed average TPM for the structure treatment of all the genes within each organism that contribute to each unique step in panel A.

a decrease in flux through the glyoxylate shunt, with more carbon being funneled through the canonical TCA cycle. In addition, over a quarter of the genes that were more highly expressed in 100% porous media versus 25% porous media were transporters (avg. base mean = 112, avg. $\log_2$ fold change = 24.2), and 62% of transporter expression was assigned to *Ensifer* (Fig. S5, Table S2). Most of the transporter genes expressed by *Ensifer* were branched-chain amino acid transporters, suggesting that in high-moisture

conditions, nitrogen is likely acquired from free peptides or necromass. However, we detected differential transcript abundance from multiple organisms (Table S4) for non-specific generalist transporters like phosphoenolpyruvate transport systems (PTSs) and glucose transporters (gtsA), which likely contributed to the acquisition of GlcNAc and glucose.

Under low-moisture conditions, we detected an increase in the expression of GH18 chitinases by *Streptomyces*. While *Streptomyces* GH18 expression was significantly lower in the 100% porous media incubations relative to liquid culture ($P \leq 0.05$), three of the four *Streptomyces*-encoded GH18s are significantly more highly expressed in the lowest moisture treatment relative to the high moisture treatment. In support of microbial communities shifting towards respiratory metabolisms under drier conditions, we observed *Sphingopyxis* to display higher expression of respiratory metabolisms related to glycolysis (acetyl-CoA synthetase [K01895] under lower moisture, which could explain its increased abundance in the community (as measured by metagenomics). Further, overall transcriptomic activity was significantly higher in the 25% saturation compared with the 100% fully saturated porous media ($t = 3.3$, $P \leq 0.05$) (Fig. S6), and our respiration measurements showed significantly higher respiration in 25% saturation ($P \leq 0.05$) (Fig. S7). Our CUE proxy also suggests a lower CUE in 25% moisture, though this difference was not significant ($P > 0.05$).

Metabolite informed metatranscriptomics suggests high expression of osmolytes, and possible biofilm genes are important bacterial responses to stress in our consortia

To understand how the different microbial expression patterns were influencing the metabolite profiles in our incubations, we collected metabolite data paired with our metatranscriptomes (Fig. S8, Table S5). We detected and annotated 138 unique known metabolites, with nearly a quarter of them being differentially abundant across our treatments. Static metabolites across treatments consisted of diverse range of molecules, though sucrose was the only sugar detected. Other metabolites included amino acids, organic acids, and aromatic compounds. Differentially abundant metabolites included compounds having roles in critical biological mechanisms, such as stress response (ectoine and trimethylamine n-oxide) (48) signaling (indole-3-acetic acid) (49), inhibition of biofilm formation (indole-3-carbaldehyde and undecanedioic acid) (50), promotion of biofilm formation (N-acetylputrescine) (51), and biofilm modification (hypoxanthine) (52).

Observed gene expression patterns explained the difference for 23 of 24 metabolites with significant differential abundance ($P \leq 0.05$). Among these metabolites were ectoine and N-acetylputrescine (Fig. 5). Sparse partial least squares (sPLS) results showed that *Ensifer* had the highest variable importance in the projection (VIP) index with regards to the predicted and observed measurements of ectoine and N-acetylputrescine. However, given that *Ensifer* was expressing genes at such a high level in the structured treatment samples, we constrained our sPLS results by examining whether *Ensifer* encoded and expressed the genetic machinery necessary to produce the predicted metabolites. The overall expression of genes that contribute to the production of ectoine and N-acetylputrescine positively correlated with the observed metabolite concentrations (Fig. 5C and F), suggesting that *Ensifer* is likely the main driver of these two metabolite concentrations, which can be important in processes like stress response (ectoine) and biofilm production (N-acetylputrescine).

DISCUSSION

Phenotypes expressed in structured habitats differ from liquid cultures

Differences in porosity and connectivity due to a structured matrix (i.e., soils) and changes in moisture can alter SOM depletion rates and reshape system chemistry (53). Reflecting this paradigm, *Streptomyces* and *Dyadobacter* showed a significant reduction

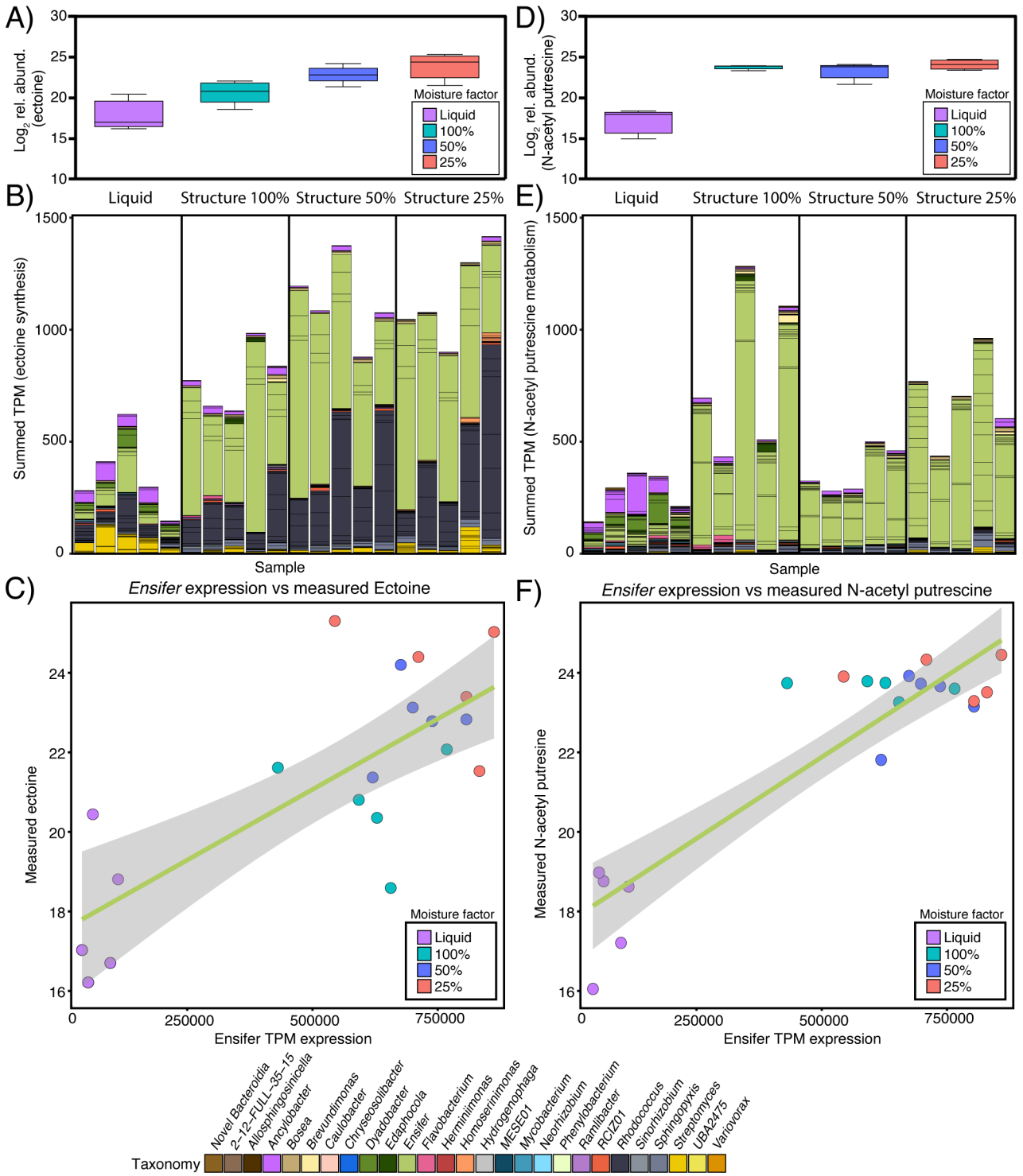

FIG 5 Ensifer is key player upon introduction structure and moisture likely due to its ability to respond to stress and possibly form biofilms. (A) Bar plots show the $\log_2$ fold change of significantly different ($P \leq 0.05$) ectoine metabolite. (B) Stacked bar chart shows the summed transcripts per million (TPM) expression of ectoine synthesis genes colored by phyla of contributing organisms. (C) sPLS shows the measured ectoine concentrations versus the overall *Ensifer* TPM expression. (D–F) Same as panels A–C but for significantly different ($P \leq 0.05$) N-acetyl putrescine metabolite.

in transcript abundance when grown in our porous media system compared to liquid (Fig. 2). In agreement with prior laboratory experiments using the model soil consortia (MSC) (16), the most highly expressed chitinase was encoded by *Streptomyces*. In fact,

Streptomyces chitinase expression is 18-fold lower in 100% porous media compared with liquid culture. Our porous media results validate observed microbial chitin degradation phenotypes in natural soils, which suggest that *Streptomyces* is a key organism of the chitin degradation phenotype (54–56). All *Streptomyces* GH18 chitinases were extracellular enzymes, thus one possible explanation for these high expression patterns in liquid culture is that chitinases (and the resulting degradation products) diffuse away in a fully liquid system and are active at high enough efficiencies to fully sustain the growth of *Streptomyces*. Since the only highly expressed chitinase in the liquid system belonged to *Streptomyces*, we suggest that it is being "cheated" out of chitin degradation products by microbial populations that do not contribute to chitin backbone decomposition (57, 58).

Community "cheaters" are prevalent in well mixed systems that do not have a physical environmental matrix (59). In support of this concept of "cheaters", we saw that *Dyadobacter* accounted for 33% of the chitin byproduct degradation (e.g., chitobiose, GlcNAc-6P, GlcN-6p) in liquid culture while contributing none of chitinase activity. Additionally, contrary to *Streptomyces* chitinase in the liquid treatment, the most expressed chitinase (GH19) in the porous media treatments was predicted to be a membrane-bound enzyme from *Ensifer*. As such, it is likely that by being membrane-bound, the chitinase yields higher concentration of privatized local chitin degradation products (i.e., chitooligomers and n-acetylglucosamine) to allow for species-specific growth, as opposed to widespread community sharing, a concept that has been previously explored (60).

The degradation of complex C polymers is a key part of ecosystem respiration and nutrient cycling and can have critical impacts on carbon storage and climate (61, 62). Specifically, organic matter degradation, including chitin, can increase concentrations of carbon dioxide and nitrous oxide (54), with implications for agricultural management and soil health. By using our reduced complexity approach, we provide evidence supporting the idea that microbial communities in complex environments like soils thrive through interactions and metabolic handoffs (63). Further, in the context of an environmental matrix (i.e., soil particles), the range of excreted proteins might be limited by diffusion, decreasing the availability of insoluble complex carbon sources like chitin. This may in part explain why the community seems to move away from chitin degradation in porous media and instead moves toward more carbon conservation mechanisms. Future work quantifying and visualizing how much carbon from chitin is shared between organisms in both reduced-complexity and natural soil systems will provide much needed constraints to models of organic matter decomposition and cycling.

Moisture, motility, and biofilm production in porous media influence community chitin degradation

In soils, changing moisture regimes exacerbate the accessibility of carbon and competition by means of selection (64–66). Further, high soil moisture often leads to depletion of oxygen (67), which can cause stress responses in microbial communities, and in turn have negative effects on soil and plant health (68). In our incubations, these soil dynamics were reflected in significantly different phenotypic responses between high moisture (100%) and low moisture (25%) conditions. These changes were underscored by an increase in overall activity as denoted by transcriptomic expression under low moisture (Fig. S6). Given that stress responses (i.e., shock proteins) were highly expressed in 100% moisture, and that overall respiration was significantly lower, our results suggest that our incubations capture relevant soil conditions and provide insights into the mechanisms of microbial survival in natural settings.

Another possible reason for the reduction of chitinase expression in porous media is that *Streptomyces* are filamentous, non-motile bacteria, and are one of thirteen bacteria in this consortium that do not have a flagellar mechanism, along with *Dyadobacter* (see the supplemental methods and results). Recent work found a positive relationship between flagellar motility mechanisms and cellular access to carbon (69), which supports the idea that the decrease in expression of *Streptomyces* (and other

non-motile organisms) is possibly due to the inability to access substrates in porous media incubations. Other work has also suggested a relationship between the ability of a cell to form flagella and produce biofilms (70), which may explain why *Ensifer* is so abundant and highly expressed in the structured incubations. Moreover, decreases in moisture content can lead to further isolation and differences in nutrient availability, and these dynamics are significant drivers of microbial processes across soil pores sizes (71) and varying hydrologic connectivity (72). Preliminary data from stained microscopy images (data not shown) suggest the *Ensifer* is a major contributor to overall biofilm production in our reduced complexity incubations. Nonetheless, further research understanding the structuring of communities around biofilms and how communities scavenge for resources in reduced complexity incubations can potentially shed light on these dynamics in soil systems.

The role that spatial structure can have on a microbial community can also go beyond substrate acquisition. A recent publication implemented an individual-based spatial simulation and found evidence that spatial segregation was induced by competition avoidance (73). Mattei and Arenas (73) propose that this competition avoidance is an important mechanism for the coexistence of microbial populations in communities. In addition to the proposed idea of metabolic "cheaters" and competition for substrates, it is likely that in structured habitats, a lack of avoidance strategies (e.g., motility) decreases the competitiveness of non-motile organisms like *Dyadobacter* and *Streptomyces*.

The degradation of chitin (and other complex carbon types) in heterogeneous environments is referred to as a "public goods dilemma" that can be solved by generating biofilms that confine goods to producers (74, 75). Previous experiments show *Ensifer* can generate biofilms (76). Further, ectoine (77) and putrescine (51) are metabolites that are commonly associated with osmotic stress and biofilm production, respectively. Since our sPLS analyses link ectoine and N-acetylputrescine synthesis to *Ensifer* gene expression, we infer that *Ensifer* is likely a key organism under soil-like stress-inducing conditions (i.e., porous media) and is likely respond to oxygen gradients, substrate availability, and metabolic cross-feeding (78). While *Ensifer* consistently surfaced as a key organism in our community, it is also likely that these phenotypes are expressed by different organisms under different conditions (i.e., *Streptomyces* may contribute more ectoine under 25% porous media, and *Rhodococcus* contributes a substantial portion of ectoine degradation pool in porous media). Moving forward, localizing the degradation of chitin within a porous media incubation (i.e., whether it occurs within a biofilm and in which layer) would help constrain the metabolic interactions that regulate decomposition in soil ecosystems. Nonetheless, these findings suggest that *Ensifer* may play a key role in the overall decomposition phenotype of soil environments through stress mitigation and biofilm production.

Microbial stress and carbon conservation responses are defining factors of overall microbial community expression patterns in porous media incubation

Due to the soil's high complexity, how microorganisms allocate carbon (79) and how bioavailability of carbon is influenced by moisture (80) are critical components of ecosystem-level dynamics. Our results showed that while respiration (i.e., CO_2 release) was highest in the liquid culture and lowest in 100% porous media, biomass (i.e., total protein detected) remained consistent across treatments, suggesting metabolic adaptation. The glyoxylate shunt plays a key role in microbial adaptation to anoxia, carbon limitation, and desiccation (81–84). Throughout both the structured vs liquid and high-moisture versus low-moisture differential expression analyses, isocitrate lyase (K01637) is the highest differentially expressed functionally annotated gene (Fig. 4). In agreement with a previous study that used qRT-PCR, isocitrate lyase, and not malate synthase, was the only glyoxylate shunt gene that was more highly expressed (83), which we hypothesize is due to regulatory signals. We also detected a decrease (but not an absence) in isocitrate lyase between the 100% and 25% moisture porous media,

suggesting a bet-hedging mechanism employed to survive which decreases (but does not shut down) canonical respiration metabolism.

In permafrost soils, researchers found that genes involved in the glyoxylate shunt were a key differentially abundant group in non-methanogenic sites and suggested that it plays a key role under conditions with thermodynamically unfavorable C substrates (85). Others argue that the glyoxylate shunt can play a key role in quiescence, which is likely highly relevant to soil systems that are prone to wetting and rewetting cycles by weather and agricultural practices (86). Our results bolster support for these hypotheses and offer a mechanistic characterization of the expression profiles of the glyoxylate shunt genes, highlighting the environmental conditions in which these phenotypes may be important.

Microorganisms are known to adapt to environmental stressors to survive under a myriad of conditions. One of these survival strategies can be the production of polyhydroxyalkanoate (PHA) carbon storage molecules, which can store carbon during times of optimal substrate availability and tap into those resources under carbon-limited, stressful conditions (87–90). The most expressed functionally annotated gene in our entire data set belongs to *Ensifer adhaerens* and is annotated as a phasin gene. Phasins are surface-binding proteins for PHA granules. Previous literature states that *Sinorhizobium*, a genus very phylogenetically close to *Ensifer*, can use its isocitrate lyase gene alongside PHA, specifically poly-β-hydroxybutyrate (PHB), from its carbon storage granules to survive in carbon-limited conditions (91). *Sinorhizobium* can also perform bet-hedging between high and low PHB-producing progeny, which enhances geometric mean fitness by producing daughter cells suited to both short-term and long-term starvation (92).

In the soil ecosystem, PHAs are a common possible carbon source (93). Ultimately, our genome-resolved analyses of a reduced complexity community enabled us to highlight a potential key role that PHAs can have in maintaining other critical microbial survival strategies (i.e., glyoxylate shunt), in response to an absence of other more favorable respiratory metabolisms (i.e., chitin degradation). Future studies that pair multi-omic measurements with visualization of PHA granules will help further untangle the underpinnings of chitin degradation in these soil-relevant conditions and provide insights into the role that PHAs can have on soil microbial phenotypes.

Reduced complexity consortia grown in porous media sheds light on microbial priming dynamics for complex carbon degradation

Given how widespread and highly expressed phasins were in our samples, we hypothesized that PHA granules might play a priming role for the overall ability of MSC-1 organisms to use chitin as a carbon source. Our reduced complexity community was cultured in natural soil extracts which contained a myriad of different possible carbon sources besides chitin, including glucose and sucrose (Table S5). Additionally, our incubations were amended with 600 ppm of glucose to stimulate microbial growth in addition to the 1,000ppm chitin. Respiration measurements from a preliminary experiment showed rapid growth patterns within 24 h, at which point we hypothesize the cells were primed to produce enzymatic machinery for chitin degradation (Fig. S9). We also hypothesize that during this high-carbon earlier stage, microbes are also producing carbon storage granules like PHA for future use.

These priming and growth constraint dynamics are well studied in soil and river hyporheic ecosystems (94–96). Specifically in soils, researchers have shown that glucose causes significant shifts in soil chemistry and antibiotic inhibition in *Streptomyces* (97). Others have also shown that in soil incubations, inputs of labile organic carbon can promote the decomposition of native soil organic matter (65). As such, we propose that for MSC-1, the overall ability to degrade chitin depends on the availability of simpler carbon substrates that can kickstart microbial metabolism. Specifically, we hypothesize that *Streptomyces* can only achieve high levels of chitin degradation in liquid systems that maximize diffusion of priming substrates and metabolic cross-feeding, or within

biofilms that can facilitate the organization and transfer of public goods. Consequently, we suspect that the observed patterns of decreased chitin degradation in the porous media condition are a combination of lack of motility, priming substrates, and suitable redox conditions, which together activate carbon conservation strategies that are more suited to those conditions (i.e., *Ensifer* glyoxylate shunt).

Recent work demonstrated a drought induced tradeoff between stress tolerance traits and resource acquisition traits (98). Induction of such strategies ultimately should alter carbon flux and energy expenditure for these organisms and would likely alter SOM decomposition rate and CUE, or the proportion of growth over carbon intake. Here, we find support for these findings using a reduced complexity model consortium and present evidence that habitat structure, and to a lesser degree moisture, induce altered community metaphenome resulting from (i) a metabolic shift to stress tolerance traits (e.g., increased production of ectoine and n-acetylputrescine), (ii) a decrease in resource acquisition traits (chitinase expression), and (iii) yield optimization via an increase in enzymes involved in carbon conservation pathways, including glyoxylate shunt and PHA utilization. Given the reproducibility of our porous media incubations, we believe that our model consortia are a great starting point for identifying metabolic and environmental control points dictating chitin decomposition, which can ultimately help constrain the soil carbon cycle.

Moving forward from laboratory-scale incubations to field-scale measurements

Even at a scale of approximately 29 different organisms, phenotypic expression was observed to be more than just the expression of biochemical pathways that these communities were enriched for (chitin degradation) and instead were observed to be a complex network of interactions related to redox conditions (i.e., oxygenation, porosity, connectivity), metabolic handoffs (i.e., community cheaters and biofilm production), and fluctuating carbon metabolisms (i.e., glyoxylate shunt, glycolysis, chitin metabolism). The complexity of these phenotypic responses are reminders of the emergent properties that arise from microbial community interactions which are difficult to track in their entirety.

The results presented here originate from an incubated reduced-complexity microcosm that may hold relevance beyond laboratory-scale experiments. Of course, soil complexity goes beyond just a pore structure; there are also microscale variations in chemistry (99), differences in ion exchange capacity (100), texture (101), and a myriad of others. Nonetheless, given the changes in expression that we see upon the introduction of a structural component (i.e., glass beads), we assert that glass–bead incubations are more reflective of soil-like conditions than liquid broth. To obtain field-relevant results, it is essential to include environmental variables, such as structure, when studying soil microbial communities, as these factors significantly influence microbial phenotypes. Ultimately, further developing experimental platforms that mimic the complexity of soil is essential for translating laboratory findings to field scales and to produce more accurate models and effective strategies for soil management and conservation.

ACKNOWLEDGMENTS

This program is supported by the U. S. Department of Energy, Office of Science, through the Genomic Science Program, Office of Biological and Environmental Research, under FWP 70880. Protein and metabolite analyses by LC-MS were performed in the William R. Wiley Environmental Molecular Sciences Laboratory (EMSL), a national scientific user facility sponsored by Office of Biological and Environmental Research and located at PNNL under EMSL project 60461: Prediction of response of microbial interaction networks cycling carbon to changing moisture conditions. PNNL is a multi-program national laboratory operated by Battelle for the DOE under Contract DE-AC05-76RLO 1830. Metagenome and metatranscriptomes were generated at the DOE Joint Genome Institute on Project 508623 under Contract No. DE-AC02-05CH11231.

Thanks go to Patricia Miller, who assisted metabolite sample preparation; Josie Eder, who analyzed the samples by LC–MS; and Isabella Yang, who assisted with metabolite identification.

AUTHOR AFFILIATION

[1]Pacific Northwest National Laboratory, Earth and Biological Sciences Directorate, Richland, Washington, USA

AUTHOR ORCIDs

Josué Rodríguez-Ramos http://orcid.org/0000-0002-2049-2765
Natalie Sadler http://orcid.org/0000-0003-1161-5687
Elias K. Zegeye http://orcid.org/0000-0002-5130-582X
Samuel Purvine http://orcid.org/0000-0002-2257-2400
Sneha Couvillion http://orcid.org/0000-0003-0307-9343
William C. Nelson http://orcid.org/0000-0002-1873-3929
Kirsten S. Hofmockel http://orcid.org/0000-0003-1586-2167

FUNDING

Funder	Grant(s)	Author(s)
Department of Energy, Office of Science, Genomic Sciences Program	FWP 70880	Kirsten S. Hofmockel
DOE | SC | PNNL | Environmental Molecular Sciences Laboratory (EMSL)	60461	Kirsten Hofmockel
Joint Genome Institute (JGI)	508623	Kirsten Hofmockel

AUTHOR CONTRIBUTIONS

Josué Rodríguez-Ramos, Conceptualization, Data curation, Formal analysis, Investigation, Methodology, Validation, Visualization, Writing – original draft, Writing – review and editing | Natalie Sadler, Conceptualization, Data curation, Formal analysis, Investigation, Methodology, Validation, Visualization, Writing – original draft, Writing – review and editing | Elias K. Zegeye, Conceptualization, Investigation, Methodology, Visualization | Yuliya Farris, Methodology | Samuel Purvine, Formal analysis, Methodology | Sneha Couvillion, Formal analysis, Methodology, Writing – original draft | William C. Nelson, Conceptualization, Investigation, Methodology, Supervision, Writing – original draft, Writing – review and editing | Kirsten S. Hofmockel, Conceptualization, Funding acquisition, Methodology, Project administration, Resources, Supervision, Writing – original draft, Writing – review and editing

DATA AVAILABILITY

All codes generated for this study are publicly available on GitHub (https://github.com/jrr-microbio/MSC1_SSA_incubations_moisture) via an R markdown document, along with full resolution supplemental figures. Raw reads, trimmed reads, and assemblies are available on the JGI IMG data portal (https://data.jgi.doe.gov/) under project IDs 1404644 to 1404648 (long-read metagenomes), 1404665 to 1404669 (short-read metagenomes), and 1404747 to 1404771 (metatranscriptomes). MAG fasta files and annotations are hosted on the PNNL DataHub under DOI 10.25584/2476507 (https://data.pnnl.gov/group/nodes/dataset/34119) (102).

ADDITIONAL FILES

The following material is available online.

Supplemental Material

Supplemental material (mSystems01616-24-S0001.docx). Supplemental methods and results, supplemental table captions, and Figures S1–S9.
Table S1 (mSystems01616-24-S0002.xlsx). MAG metadata, including quality and read mapping results.
Table S2 (mSystems01616-24-S0003.xlsx). MAG metabolism heatmaps.
Table S3 (mSystems01616-24-S0004.xlsx). Highlighted metabolisms within the paper.
Table S4 (mSystems01616-24-S0005.xlsx). Differential expression analysis output.
Table S5 (mSystems01616-24-S0006.xlsx). Metabolite data.
Table S6 (mSystems01616-24-S0007.xlsx). DRAM metabolism summaries.

REFERENCES

1. Jin C, Sengupta A. 2024. Microbes in porous environments: from active interactions to emergent feedback. Biophys Rev 16:173–188. https://doi.org/10.1007/s12551-024-01185-7
2. Ebrahimi A, Or D. 2015. Hydration and diffusion processes shape microbial community organization and function in model soil aggregates. Water Resour Res 51:9804–9827. https://doi.org/10.1002/2015WR017565
3. Pett-Ridge J, Firestone MK. 2005. Redox fluctuation structures microbial communities in a wet tropical soil. Appl Environ Microbiol 71:6998–7007. https://doi.org/10.1128/AEM.71.11.6998-7007.2005
4. Elieh-Ali-Komi D, Hamblin MR. 2016. Chitin and chitosan: production and application of versatile biomedical nanomaterials. Int J Adv Res 4:411–427.
5. Merzendorfer H. 2006. Insect chitin synthases: a review. J Comp Physiol B 176:1–15. https://doi.org/10.1007/s00360-005-0005-3
6. Wieczorek AS, Schmidt O, Chatzinotas A, von Bergen M, Gorissen A, Kolb S. 2019. Ecological functions of agricultural soil bacteria and microeukaryotes in chitin degradation: a case study. Front Microbiol 10:1293. https://doi.org/10.3389/fmicb.2019.01293
7. Dechesne A, Wang G, Gülez G, Or D, Smets BF. 2010. Hydration-controlled bacterial motility and dispersal on surfaces. Proc Natl Acad Sci USA 107:14369–14372. https://doi.org/10.1073/pnas.1008392107
8. Smercina DN, Bailey VL, Hofmockel KS. 2021. Micro on a macroscale: relating microbial-scale soil processes to global ecosystem function. FEMS Microbiol Ecol 97:fiab091. https://doi.org/10.1093/femsec/fiab091
9. Schimel JP, Schaeffer SM. 2012. Microbial control over carbon cycling in soil. Front Microbiol 3:348. https://doi.org/10.3389/fmicb.2012.00348
10. Malik AA, Martiny JBH, Brodie EL, Martiny AC, Treseder KK, Allison SD. 2020. Defining trait-based microbial strategies with consequences for soil carbon cycling under climate change. ISME J 14:1–9. https://doi.org/10.1038/s41396-019-0510-0
11. Beier S, Bertilsson S. 2013. Bacterial chitin degradation-mechanisms and ecophysiological strategies. Front Microbiol 4:149. https://doi.org/10.3389/fmicb.2013.00149
12. Karlsen ST, Rau MH, Sánchez BJ, Jensen K, Zeidan AA. 2023. From genotype to phenotype: computational approaches for inferring microbial traits relevant to the food industry. FEMS Microbiol Rev 47:fuad030. https://doi.org/10.1093/femsre/fuad030
13. Salt GW. 1979. A comment on the use of the term emergent properties. Am Nat 113:145–148. https://doi.org/10.1086/283370
14. Hall EK, Bernhardt ES, Bier RL, Bradford MA, Boot CM, Cotner JB, Del Giorgio PA, Evans SE, Graham EB, Jones SE, Lennon JT, Locey KJ, Nemergut D, Osborne BB, Rocca JD, Schimel JP, Waldrop MP, Wallenstein MD. 2018. Understanding how microbiomes influence the systems they inhabit. Nat Microbiol 3:977–982. https://doi.org/10.1038/s41564-018-0201-z
15. McClure R, Naylor D, Farris Y, Davison M, Fansler SJ, Hofmockel KS, Jansson JK. 2020. Development and analysis of a stable, reduced complexity model soil microbiome. Front Microbiol 11:1987. https://doi.org/10.3389/fmicb.2020.01987
16. McClure R, Farris Y, Danczak R, Nelson W, Song H-S, Kessell A, Lee J-Y, Couvillion S, Henry C, Jansson JK, Hofmockel KS. 2022. Interaction networks are driven by community-responsive phenotypes in a chitin-degrading consortium of soil microbes. mSystems 7:e0037222. https://doi.org/10.1128/msystems.00372-22
17. McClure R, Garcia M, Couvillion S, Farris Y, Hofmockel KS. 2022. Removal of primary nutrient degraders reduces growth of soil microbial communities with genomic redundancy. Front Microbiol 13:1046661. https://doi.org/10.3389/fmicb.2022.1046661
18. Sparling GP, West AW. 1990. A comparison of gas chromatography and differential respirometer methods to measure soil respiration and to estimate the soil microbial biomass. Pedobiologia 34:103–112. https://doi.org/10.1016/S0031-4056(24)00013-1
19. Rouwenhorst RJ, Jzn JF, Scheffers WA, van Dijken JP. 1991. Determination of protein concentration by total organic carbon analysis. J Biochem Biophys Methods 22:119–128. https://doi.org/10.1016/0165-022x(91)90024-q
20. Neidhardt FC, Ingraham JL, Schaechter M. 1990. Physiology of the bacterial cell: a molecular approach. Sinauer Associates, Sunderland, MA.
21. Clum A, Huntemann M, Bushnell B, Foster B, Foster B, Roux S, Hajek PP, Varghese N, Mukherjee S, Reddy TBK, Daum C, Yoshinaga Y, O'Malley R, Seshadri R, Kyrpides NC, Eloe-Fadrosh EA, Chen I-MA, Copeland A, Ivanova NN. 2021. DOE JGI metagenome workflow. mSystems 6:e00804-20. https://doi.org/10.1128/mSystems.00804-20
22. Bushnell B. BBMap: A Fast, Accurate, Splice-Aware Aligner. LBNL-7065E; Lawrence Berkeley National Lab (LBNL), Berkeley, CA (United States)
23. Li D, Liu C-M, Luo R, Sadakane K, Lam T-W. 2015. MEGAHIT: an ultra-fast single-node solution for large and complex metagenomics assembly via succinct *de Bruijn* graph . Bioinformatics 31:1674–1676. https://doi.org/10.1093/bioinformatics/btv033
24. Seemann T. 2018. Barrnap (0.9). github. Available from: https://github.com/tseemann/barrnap
25. Uritskiy GV, DiRuggiero J, Taylor J. 2018. MetaWRAP-a flexible pipeline for genome-resolved metagenomic data analysis. Microbiome 6:158. https://doi.org/10.1186/s40168-018-0541-1
26. Shen W, Le S, Li Y, Hu F. 2016. SeqKit: a cross-platform and ultrafast toolkit for FASTA/Q file manipulation. PLoS ONE 11:e0163962. https://doi.org/10.1371/journal.pone.0163962
27. Bowers RM, Kyrpides NC, Stepanauskas R, Harmon-Smith M, Doud D, Reddy TBK, Schulz F, Jarett J, Rivers AR, Eloe-Fadrosh EA. 2017. Minimum information about a single amplified genome (MISAG) and a metagenome-assembled genome (MIMAG) of bacteria and archaea. Nat Biotechnol 35:725–731. https://doi.org/10.1038/nbt.3893
28. Shaffer M, Borton MA, McGivern BB, Zayed AA, La Rosa SL, Solden LM, Liu P, Narrowe AB, Rodríguez-Ramos J, Bolduc B, Gazitúa MC, Daly RA, Smith GJ, Vik DR, Pope PB, Sullivan MB, Roux S, Wrighton KC. 2020. DRAM for distilling microbial metabolism to automate the curation of microbiome function. Nucleic Acids Res 48:8883–8900. https://doi.org/10.1093/nar/gkaa621
29. Cantalapiedra CP, Hernández-Plaza A, Letunic I, Bork P, Huerta-Cepas J. 2021. EggNOG-mapper v2: functional annotation, orthology assignments, and domain prediction at the metagenomic scale. Mol Biol Evol 38:5825–5829. https://doi.org/10.1093/molbev/msab293
30. Chaumeil P-A, Mussig AJ, Hugenholtz P, Parks DH. 2019. GTDB-Tk: a toolkit to classify genomes with the genome taxonomy database. Bioinformatics 36:1925–1927. https://doi.org/10.1093/bioinformatics/btz848
31. Parks DH, Chuvochina M, Waite DW, Rinke C, Skarshewski A, Chaumeil P-A, Hugenholtz P. 2018. A standardized bacterial taxonomy based on genome phylogeny substantially revises the tree of life. Nat Biotechnol 36:996–1004. https://doi.org/10.1038/nbt.4229

32. Yu NY, Wagner JR, Laird MR, Melli G, Rey S, Lo R, Dao P, Sahinalp SC, Ester M, Foster LJ, Brinkman FSL. 2010. PSORTb 3.0: improved protein subcellular localization prediction with refined localization subcategories and predictive capabilities for all prokaryotes. Bioinformatics 26:1608–1615. https://doi.org/10.1093/bioinformatics/btq249
33. Woodcroft BJ. 2022. Github. CoverM: read coverage calculator for metagenomics. Available from: https://github.com/wwood/CoverM
34. Liao Y, Smyth GK, Shi W. 2014. featureCounts: an efficient general purpose program for assigning sequence reads to genomic features. Bioinformatics 30:923–930. https://doi.org/10.1093/bioinformatics/btt656
35. 2024. Package recipe "subread" — bioconda documentation. Available from: https://bioconda.github.io/recipes/subread/README.html
36. Smid M, Coebergh van den Braak RRJ, van de Werken HJG, van Riet J, van Galen A, de Weerd V, van der Vlugt-Daane M, Bril SI, Lalmahomed ZS, Kloosterman WP, Wilting SM, Foekens JA, IJzermans JNM, Martens JWM, Sieuwerts AM, MATCH study group. 2018. Gene length corrected trimmed mean of M-values (GeTMM) processing of RNA-seq data performs similarly in intersample analyses while improving intrasample comparisons. BMC Bioinformatics 19:236. https://doi.org/10.1186/s12859-018-2246-7
37. Love MI, Huber W, Anders S. 2014. Moderated estimation of fold change and dispersion for RNA-seq data with DESeq2. Genome Biol 15:550. https://doi.org/10.1186/s13059-014-0550-8
38. OksanenJ, BlanchetFG, FriendlyM, LegendreP, McGlinn D, MinchinPR, O'haraRB, SimpsonGL. 2016. Vegan: community ecology package. R Foundation for Statistical Computing, Vienna.
39. Chung D, Chun H, Keles S. 2012. SPLS: sparse partial least squares (SPLS) regression and classification. R package version 2:1.
40. Wickham H. 2016. *Ggplot2: Elegant Graphics for Data Analysis*. Springer-Verlag New York.
41. Mauri M, Elli T, Caviglia G, Uboldi G, Azzi M. 2017. RAWGraphs: a visualisation platform to create open outputs, p 1–5Association for Computing Machinery, New York, NY, USA
42. Chambers MC, Maclean B, Burke R, Amodei D, Ruderman DL, Neumann S, Gatto L, Fischer B, Pratt B, Egertson J. 2012. A cross-platform toolkit for mass spectrometry and proteomics. Nat Biotechnol 30:918–920. https://doi.org/10.1038/nbt.2377
43. Gibbons BC, Chambers MC, Monroe ME, Tabb DL, Payne SH. 2015. Correcting systematic bias and instrument measurement drift with mzRefinery. Bioinformatics 31:3838–3840. https://doi.org/10.1093/bioinformatics/btv437
44. Elias JE, Gygi SP. 2007. Target-decoy search strategy for increased confidence in large-scale protein identifications by mass spectrometry. Nat Methods 4:207–214. https://doi.org/10.1038/nmeth1019
45. Tsugawa H, Ikeda K, Takahashi M, Satoh A, Mori Y, Uchino H, Okahashi N, Yamada Y, Tada I, Bonini P, Higashi Y, Okazaki Y, Zhou Z, Zhu Z-J, Koelmel J, Cajka T, Fiehn O, Saito K, Arita M, Arita M. 2020. A lipidome atlas in MS-DIAL 4. Nat Biotechnol 38:1159–1163. https://doi.org/10.1038/s41587-020-0531-2
46. Stratton KG, Claborne DM, Degnan DJ, Richardson RE, White AM, McCue LA, Webb-Robertson B-JM, Bramer LM. 2024. PMart web application: marketplace for interactive analysis of panomics data. J Proteome Res 23:3310–3317. https://doi.org/10.1021/acs.jproteome.3c00512
47. Holm S. 1979. A simple sequentially rejective multiple test procedure. Scand J Stat 6:65–70.
48. Nazarov AV, Anan'ina LN, Gorbunov AA, Pyankova AA. 2022. Bacteria producing ectoine in the rhizosphere of plants growing on technogenic saline soil. Eurasian Soil Sc 55:1074–1081. https://doi.org/10.1134/S1064229322080129
49. Keswani C, Singh SP, Cueto L, García-Estrada C, Mezaache-Aichour S, Glare TR, Borriss R, Singh SP, Blázquez MA, Sansinenea E. 2020. Auxins of microbial origin and their use in agriculture. Appl Microbiol Biotechnol 104:8549–8565. https://doi.org/10.1007/s00253-020-10890-8
50. Jin X, Zhou J, Richey G, Wang M, Hong SMC, Hong SH. 2021. Undecanoic acid, lauric acid, and N-tridecanoic acid inhibit *Escherichia coli* persistence and biofilm formation. J Microbiol Biotechnol 31:130–136. https://doi.org/10.4014/jmb.2008.08027
51. Liu Z, Hossain SS, Morales Moreira Z, Haney CH. 2022. Putrescine and its metabolic precursor arginine promote biofilm and c-di-GMP synthesis in *Pseudomonas aeruginosa*. J Bacteriol 204:e00297-21. https://doi.org/10.1128/JB.00297-21
52. Gallegos-Monterrosa R, Kankel S, Götze S, Barnett R, Stallforth P, Kovács ÁT. 2017. *Lysinibacillus fusiformis* M5 induces increased complexity in *Bacillus subtilis* 168 colony biofilms via hypoxanthine. J Bacteriol 199:e00204-17. https://doi.org/10.1128/JB.00204-17
53. Rezanezhad F, Couture R-M, Kovac R, O'Connell D, Van Cappellen P. 2014. Water table fluctuations and soil biogeochemistry: an experimental approach using an automated soil column system. J Hydrol (Amst) 509:245–256. https://doi.org/10.1016/j.jhydrol.2013.11.036
54. Hui C, Jiang H, Liu B, Wei R, Zhang Y, Zhang Q, Liang Y, Zhao Y. 2020. Chitin degradation and the temporary response of bacterial chitinolytic communities to chitin amendment in soil under different fertilization regimes. Sci Total Environ 705:136003. https://doi.org/10.1016/j.scitotenv.2019.136003
55. Wang J-L, Chen Y-C, Deng J-J, Mo Z-Q, Zhang M-S, Yang Z-D, Zhang J-R, Li Y-W, Dan X-M, Luo X-C. 2023. Synergic chitin degradation by *Streptomyces* sp. SCUT-3 chitinases and their applications in chitinous waste recycling and pathogenic fungi biocontrol. Int J Biol Macromol 225:987–996. https://doi.org/10.1016/j.ijbiomac.2022.11.161
56. Iwasaki Y, Ichino T, Saito A. 2020. Transition of the bacterial community and culturable chitinolytic bacteria in chitin-treated upland soil: from *Streptomyces* to methionine-auxotrophic Lysobacter and other genera. Microbes Environ 35:ME19070. https://doi.org/10.1264/jsme2.ME19070
57. Jacquiod S, Franqueville L, Cécillon S, Vogel TM, Simonet P. 2013. Soil bacterial community shifts after chitin enrichment: an integrative metagenomic approach. PLoS ONE 8:e79699. https://doi.org/10.1371/journal.pone.0079699
58. Beier S, Bertilsson S. 2011. Uncoupling of chitinase activity and uptake of hydrolysis products in freshwater bacterioplankton. Limnol Oceanogr 56:1179–1188. https://doi.org/10.4319/lo.2011.56.4.1179
59. Allison SD, Lu L, Kent AG, Martiny AC. 2014. Extracellular enzyme production and cheating in *Pseudomonas fluorescens* depend on diffusion rates. Front Microbiol 5:169. https://doi.org/10.3389/fmicb.2014.00169
60. Andersen SB, Ghoul M, Marvig RL, Lee Z-B, Molin S, Johansen HK, Griffin AS. 2018. Privatisation rescues function following loss of cooperation. Elife 7:e38594. https://doi.org/10.7554/eLife.38594
61. Tao F, Huang Y, Hungate BA, Manzoni S, Frey SD, Schmidt MWI, Reichstein M, Carvalhais N, Ciais P, Jiang L. 2023. Microbial carbon use efficiency promotes global soil carbon storage. Nature New Biol 618:981–985. https://doi.org/10.1038/s41586-023-06042-3
62. Jansson JK, Hofmockel KS. 2020. Soil microbiomes and climate change. Nat Rev Microbiol 18:35–46. https://doi.org/10.1038/s41579-019-0265-7
63. Hug LA, Co R. 2018. It takes a village: microbial communities thrive through interactions and metabolic handoffs. mSystems 3:e00152-17. https://doi.org/10.1128/mSystems.00152-17
64. Avila CCE, Schaefer MV, Duro AM, Haensel TP, Garniwan A, Lin Y, Darrel Jenerette G, Nico PS, Dubinsky E, Keiluweit M, Brodie EL, Lin Y-H, Homyak PM, Ying SC. 2023. Carbon dynamics as a function of soil moisture following repeated wet-dry cycles in irrigated soils. Geoderma 439:116681. https://doi.org/10.1016/j.geoderma.2023.116681
65. Bian H, Li C, Zhu J, Xu L, Li M, Zheng S, He N. 2022. Soil moisture affects the rapid response of microbes to labile organic C addition. Front Ecol Evol 10:857185. https://doi.org/10.3389/fevo.2022.857185
66. West JR, Whitman T. 2022. Disturbance by soil mixing decreases microbial richness and supports homogenizing community assembly processes. FEMS Microbiol Ecol 98:fiac089. https://doi.org/10.1093/femsec/fiac089
67. Kaur G, Singh G, Motavalli PP, Nelson KA, Orlowski JM, Golden BR. 2020. Impacts and management strategies for crop production in waterlogged or flooded soils: a review. Agron J 112:1475–1501. https://doi.org/10.1002/agj2.20093
68. Tyagi A, Ali S, Mir RA, Sharma S, Arpita K, Almalki MA, Mir ZA. 2024. Uncovering the effect of waterlogging stress on plant microbiome and disease development: current knowledge and future perspectives. Front Plant Sci 15:1407789. https://doi.org/10.3389/fpls.2024.1407789
69. Ramoneda J, Fan K, Lucas JM, Chu H, Bissett A, Strickland MS, Fierer N. 2024. Ecological relevance of flagellar motility in soil bacterial communities. ISME J 18:wrae067. https://doi.org/10.1093/ismejo/wrae067
70. Mookherjee A, Mitra M, Sason G, Jose PA, Martinenko M, Pietrokovski S, Jurkevitch E. 2024. Flagellar stator genes control a trophic shift from obligate to facultative predation and biofilm formation in a bacterial predator. mBio 15:e00715-24. https://doi.org/10.1128/mbio.00715-24

71. Li Z, Kravchenko AN, Cupples A, Guber AK, Kuzyakov Y, Philip Robertson G, Blagodatskaya E. 2024. Composition and metabolism of microbial communities in soil pores. Nat Commun 15:3578. https://doi.org/10.1038/s41467-024-47755-x
72. Bailey VL, Smith AP, Tfaily M, Fansler SJ, Bond-Lamberty B. 2017. Differences in soluble organic carbon chemistry in pore waters sampled from different pore size domains. Soil Biology and Biochemistry 107:133–143. https://doi.org/10.1016/j.soilbio.2016.11.025
73. Mattei M, Arenas A. 2024. Exploring spatial segregation induced by competition avoidance as driving mechanism for emergent coexistence in microbial communities. Phys Rev E 110:014404. https://doi.org/10.1103/PhysRevE.110.014404
74. Drescher K, Nadell CD, Stone HA, Wingreen NS, Bassler BL. 2014. Solutions to the public goods dilemma in bacterial biofilms. Curr Biol 24:50–55. https://doi.org/10.1016/j.cub.2013.10.030
75. Mukherjee S, Bassler BL. 2019. Bacterial quorum sensing in complex and dynamically changing environments. Nat Rev Microbiol 17:371–382. https://doi.org/10.1038/s41579-019-0186-5
76. Fagorzi C, Ilie A, Decorosi F, Cangioli L, Viti C, Mengoni A, diCenzo GC. 2020. Symbiotic and nonsymbiotic members of the genus Ensifer (syn. Sinorhizobium) are separated into two clades based on comparative genomics and high-throughput phenotyping. Genome Biol Evol 12:2521–2534. https://doi.org/10.1093/gbe/evaa221
77. Czech L, Hermann L, Stöveken N, Richter AA, Höppner A, Smits SHJ, Heider J, Bremer E. 2018. Role of the extremolytes ectoine and hydroxyectoine as stress protectants and nutrients: genetics, phylogenomics, biochemistry, and structural analysis. Genes (Basel) 9:177. https://doi.org/10.3390/genes9040177
78. Evans CR, Kempes CP, Price-Whelan A, Dietrich LEP. 2020. Metabolic heterogeneity and cross-feeding in bacterial multicellular systems. Trends Microbiol 28:732–743. https://doi.org/10.1016/j.tim.2020.03.008
79. Honeker LK, Pugliese G, Ingrisch J, Fudyma J, Gil-Loaiza J, Carpenter E, Singer E, Hildebrand G, Shi L, Hoyt DW. 2023. Drought re-routes soil microbial carbon metabolism towards emission of volatile metabolites in an artificial tropical rainforest. Nat Microbiol 8:1480–1494. https://doi.org/10.1038/s41564-023-01432-9
80. Heckman KA, Possinger AR, Badgley BD, Bowman MM, Gallo AC, Hatten JA, Nave LE, SanClements MD, Swanston CW, Weiglein TL, Wieder WR, Strahm BD. 2023. Moisture-driven divergence in mineral-associated soil carbon persistence. Proc Natl Acad Sci USA 120:e2210044120. https://doi.org/10.1073/pnas.2210044120
81. Ahn S, Jung J, Jang I-A, Madsen EL, Park W. 2016. Role of glyoxylate shunt in oxidative stress response. J Biol Chem 291:11928–11938. https://doi.org/10.1074/jbc.M115.708149
82. Chew SY, Chee WJY, Than LTL. 2019. The glyoxylate cycle and alternative carbon metabolism as metabolic adaptation strategies of *Candida glabrata*: perspectives from *Candida albicans* and *Saccharomyces cerevisiae*. J Biomed Sci 26:52. https://doi.org/10.1186/s12929-019-0546-5
83. Jeon J-M, Lee H-I, Sadowsky MJ, Sugawara M, Chang W-S. 2015. Characterization of a functional role of the *Bradyrhizobium japonicum* isocitrate lyase in desiccation tolerance. Int J Mol Sci 16:16695–16709. https://doi.org/10.3390/ijms160716695
84. Qi Z, Sun N, Liu C. 2023. Glyoxylate cycle maintains the metabolic homeostasis of *Pseudomonas aeruginosa* in viable but nonculturable state induced by chlorine stress. Microbiol Res 270:127341. https://doi.org/10.1016/j.micres.2023.127341
85. Waldrop MP, Chabot CL, Liebner S, Holm S, Snyder MW, Dillon M, Dudgeon SR, Douglas TA, Leewis M-C, Walter Anthony KM, McFarland JW, Arp CD, Bondurant AC, Taş N, Mackelprang R. 2023. Permafrost microbial communities and functional genes are structured by latitudinal and soil geochemical gradients. ISME J 17:1224–1235. https://doi.org/10.1038/s41396-023-01429-6
86. Chodkowski JL, Shade A. 2020. Exometabolite dynamics over stationary phase reveal strain-specific responses. mSystems 5:e00493-20. https://doi.org/10.1128/mSystems.00493-20
87. Mezzina MP, Wetzler DE, Catone MV, Bucci H, Di Paola M, Pettinari MJ. 2014. A phasin with many faces: structural insights on PhaP from Azotobacter sp. FA8. PLoS ONE 9:e103012. https://doi.org/10.1371/journal.pone.0103012
88. Sudesh K, Abe H, Doi Y. 2000. Synthesis, structure and properties of polyhydroxyalkanoates: biological polyesters. Prog Polym Sci 25:1503–1555. https://doi.org/10.1016/S0079-6700(00)00035-6
89. Obruca S, Sedlacek P, Slaninova E, Fritz I, Daffert C, Meixner K, Sedrlova Z, Koller M. 2020. Novel unexpected functions of PHA granules. Appl Microbiol Biotechnol 104:4795–4810. https://doi.org/10.1007/s00253-020-10568-1
90. Kadouri D, Jurkevitch E, Okon Y, Castro-Sowinski S. 2005. Ecological and agricultural significance of bacterial polyhydroxyalkanoates. Crit Rev Microbiol 31:55–67. https://doi.org/10.1080/10408410590899228
91. Ramírez-Trujillo JA, Dunn MF, Suárez-Rodríguez R, Hernández-Lucas I. 2016. The *Sinorhizobium meliloti* glyoxylate cycle enzyme isocitrate lyase (AceA) is required for the utilization of poly-β-hydroxybutyrate during carbon starvation. Ann Microbiol 66:921–924. https://doi.org/10.1007/s13213-015-1131-0
92. Ratcliff WC, Denison RF. 2010. Individual-level bet hedging in the bacterium *Sinorhizobium meliloti*. Curr Biol 20:1740–1744. https://doi.org/10.1016/j.cub.2010.08.036
93. Fernandes M, Salvador A, Alves MM, Vicente AA. 2020. Factors affecting polyhydroxyalkanoates biodegradation in soil. Polym Degrad Stab 182:109408. https://doi.org/10.1016/j.polymdegradstab.2020.109408
94. Bastida F, García C, Fierer N, Eldridge DJ, Bowker MA, Abades S, Alfaro FD, Asefaw Berhe A, Cutler NA, Gallardo A. 2019. Global ecological predictors of the soil priming effect. Nat Commun 10:3481. https://doi.org/10.1038/s41467-019-11472-7
95. Stegen JC, Johnson T, Fredrickson JK, Wilkins MJ, Konopka AE, Nelson WC, Arntzen EV, Chrisler WB, Chu RK, Fansler SJ, Graham EB, Kennedy DW, Resch CT, Tfaily M, Zachara J. 2018. Influences of organic carbon speciation on hyporheic corridor biogeochemistry and microbial ecology. Nat Commun 9:585. https://doi.org/10.1038/s41467-018-02922-9
96. Balakrishnan R, de Silva RT, Hwa T, Cremer J. 2021. Suboptimal resource allocation in changing environments constrains response and growth in bacteria. Mol Syst Biol 17:e10597. https://doi.org/10.15252/msb.202110597
97. Dundore-Arias JP, Castle SC, Felice L, Dill-Macky R, Kinkel LL. 2019. Carbon amendments influence composition and functional capacities of indigenous soil microbiomes. Front Mol Biosci 6:151. https://doi.org/10.3389/fmolb.2019.00151
98. Malik AA, Martiny JBH, Ribeiro A, Sheridan PO, Weihe C, Brodie EL, Allison SD. 2024. Bacterial population-level trade-offs between drought tolerance and resource acquisition traits impact decomposition. Ecology. https://doi.org/10.1101/2024.06.22.600187
99. Keiluweit M, Wanzek T, Kleber M, Nico P, Fendorf S. 2017. Anaerobic microsites have an unaccounted role in soil carbon stabilization. Nat Commun 8:1771. https://doi.org/10.1038/s41467-017-01406-6
100. Fang K, Kou D, Wang G, Chen L, Ding J, Li F, Yang G, Qin S, Liu L, Zhang Q, Yang Y. 2017. Decreased soil cation exchange capacity across northern China's grasslands over the last three decades. JGR Biogeosciences 122:3088–3097. https://doi.org/10.1002/2017JG003968
101. Shao M, Zhang S, Niu B, Pei Y, Song S, Lei T, Yun H. 2022. Soil texture influences soil bacterial biomass in the permafrost-affected alpine desert of the Tibetan plateau. Front Microbiol 13:1007194. https://doi.org/10.3389/fmicb.2022.1007194
102. Rodríguez R, Natalie S, Elias K, Yuliya F, Samuel P, Sneha C, William CN, Kirsten H. 2024. Environmental matrix and moisture are key determinants of microbial phenotypes expressed in a reduced complexity soil-analog. PNNL DataHub. Available from: https://doi.org/10.25584/2476507